A Critical Review of Heat and Mass Transfer Correlations for LiBr-H 2 O and NH 3 -H 2 O Absorption Refrigeration Machines Using Falling Liquid Film Technology

Beethoven Narváez-Romo, Marx Chhay, Elí Zavaleta-Aguilar, José R Simões-Moreira

▶ **To cite this version:**

Beethoven Narváez-Romo, Marx Chhay, Elí Zavaleta-Aguilar, José R Simões-Moreira. A Critical Review of Heat and Mass Transfer Correlations for LiBr-H 2 O and NH 3 -H 2 O Absorption Refrigeration Machines Using Falling Liquid Film Technology. Applied Thermal Engineering, 2017, 10.1016/j.applthermaleng.2017.05.092 . hal-01527189

HAL Id: hal-01527189

https://hal.univ-grenoble-alpes.fr/hal-01527189

Submitted on 24 May 2017

HAL is a multi-disciplinary open access archive for the deposit and dissemination of scientific research documents, whether they are published or not. The documents may come from teaching and research institutions in France or abroad, or from public or private research centers.

L'archive ouverte pluridisciplinaire **HAL**, est destinée au dépôt et à la diffusion de documents scientifiques de niveau recherche, publiés ou non, émanant des établissements d'enseignement et de recherche français ou étrangers, des laboratoires publics ou privés.

A Critical Review of Heat and Mass Transfer Correlations for $LiBr - H_2O$ and $NH_3 - H_2O$ Absorption Refrigeration Machines Using Falling Liquid Film Technology.

Beethoven Narváez-Romo[a], Marx Chhay[b], Elí W. Zavaleta-Aguilar[c], José R. Simões-Moreira*[a]

[a]*SISEA-Alternative Energy Systems Laboratory, Av. Professor Mello Moraes, 2231 - Cidade Universitária - São Paulo - Brazil*
[b]*LOCIE-Laboratoire Optimisation de la Conception et Ingénierie de l'Environnement Université Savoie Mont Blanc, 73376 Le Bourget-du-Lac, France*
[c]*São Paulo State University (Unesp), Campus of Itapeva, Rua Geraldo Alckmin, 519, 18409-010 - Itapeva- São Paulo - Brazil*

Abstract

This paper presents an extensive review of heat and mass transfer correlations in the framework of sorption machines operating based on the falling film technology, in which ammonia-water and lithium bromide-water are used as the working fluid pairs. Heat and mass transfer correlations (Nu, Sh) as functions of falling liquid film flow regime (Re) are summarized as well as the application range and geometrical configuration. In order to compare the correlations found in the recent and classical literature, graphs were constructed for comparing purposes of those correlations trends within the application range of absorption refrigeration machines.

Keywords: Falling film, Absorption, Review, Ammonia-Water, Lithium Bromide-Water

*Corresponding author: e-mail: jrsimoes@usp.br. SISEA/ Mechanical Engineering Department/ Escola Politécnica, University of São Paulo, Av. Professor Mello Moraes, 2231, CEP: 05508-900, São Paulo, Brazil.

Contents

1. Introduction

Edmond Carré developed the first absorption refrigeration machine in 1850 using a water and sulphuric acid (H_2SO_4) mixture as the working fluid pair, requiring a large quantity of this acid to absorb a small quantity of water vapor in order to achieve the refrigeration process. However, in 1859, Ferdinand Carré used the ammonia-water pair as working fluid, because of its properties: stability, low normal boiling point ($44°C$), and good ammonia affinity to water [1]. Currently, lithium bromide-water and ammonia-water pairs have been the most common working fluid pairs used in commercial absorption refrigeration cycles (ARC). The former operates in vacuum such as in Edmond Carré's machine, and the second one in a positive pressure such as in Ferdinand Carré 's machine.

An ARC is constituted by two pressure levels as depicted in Fig. (1); the low pressure level (evaporator and absorber) and the high pressure level (generator and condenser). These two levels are connected by two expansion valves (EV1 and EV2) and one solution pump, in its simplest configuration. The solution pump drives the strong liquid solution from the absorber to the generator in ammonia-water technology (or the weak liquid solution for the lithium bromide-water solution). At the generator, the solution flows over heated surface in the falling film generator, whose function is to separate the refrigerant (ammonia

or water vapor) from the liquid solution. Next, the vapor refrigerant is driven to the condenser, rejecting the heat to the environment, $\dot{Q}_{con}$. The condensed refrigerant reaches the evaporator, going through an expansion valve (EV2) reducing the pressure and the temperature by the Joule-Thomson effect to receive the heat load ($\dot{Q}_{eva}$) by evaporation. Next, the vapor refrigerant enters the absorber at the vapor state, in which it is absorbed by the weak solution (or strong for lithium bromide-water solution). Heat ($\dot{Q}_{abs}$) is rejected to an external coolant as the absorption process takes place, and then the solution is pumped to the generator closing the cycle.

It is worth mentioning that both the absorber and the generator are the main components of the absorption system because that there is a simultaneous heat and mass transfer process [2], in which the refrigerant changes phase [3]. In addition, the heat and mass transfer coefficients in those components are characterized by low values [4]. On the other hand, when ARC is compared with a vapor compression cycle (VCC), the former has lower coefficient of performance (COP), particularly if the absorption machine works beyond its design specifications, e.g. the vaporization temperature, or the cooling thermal load, due to a problem of partial evaporation at the evaporator. Additionally, the COP is also sensitive to the heat source temperature in the desorber, the cooling temperature of the evaporator, and flow rate of the strong solution. Therefore, enhancing the heat and mass transfer process leads to a reduction in costs and in the sorption machine size.

A heat transfer review of falling film of single component has been studied by severals researchers. Thome [5] carried out a review of falling film evaporation on both smooth and enhanced tubes focusing on working fluids as alternative refrigerants including ammonia; he found that the falling film technology provides a higher heat transfer coefficient than flooded evaporators. Killion and Garimella [6] carried out a complete critical review of falling film technology in absorption processes, in which these efforts were focused analyzing the mathematical model that have been used to the simultaneous heat and mass transfer processes. Ribatski and Jacobi [7] carried out a critical review of falling film

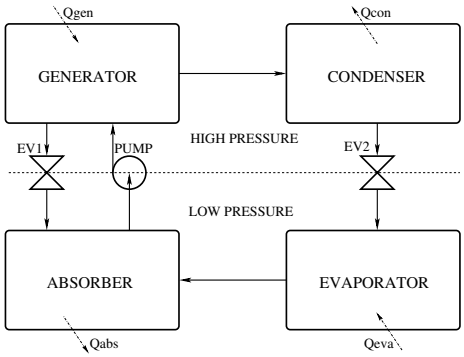

Figure 1: ARC Diagram

evaporation process over horizontal tubes (single and tube bundles), covering hydrodynamic studies and the heat transfer coefficient affected by several operation conditions on smooth and enhanced tubes. They pointed out that the falling film technology presents inconveniences due the liquid film maldistribution and dry-out problems. However, the installation of a wire mesh over the distributor homogenized the liquid flow and guaranteed the total wettability over the first tube [8]. Prost et al. [9] analyzed the heat transfer behavior falling film evaporator under several operation conditions for the food industry. They reported some Nusselt number correlations from the literature. Narváez-Romo and Simões-Moreira [10] carried out a literature review of falling film evaporation, studying the parameters affecting the heat transfer coefficient. Tomforde and Luke [11] carried out a review over falling film absorbers focused to horizontal tubes only, in which lithium bromide-water, and R134a-Dimethylacetamide (DMAC) were the working fluid pair studied.

The falling film technology has widely been studied, existing several works focused on the heat and mass transfer analysis for this technology applied to an ARC. However, we have found an opportunity to emphasize over the agreement between numerical and experimental studies based on the correlations that researchers have been obtained. Therefore, the objective of this paper is to review all the correlations of the heat and mass transfer in falling film technology carried out in sorption processes for the two most common working fluid pairs;

ammonia-water and lithium bromide-water. In the first place, a review of the mean definition correlations and the classical hypothesis assumed to compute the heat and mass transfer coefficients are presented. Next sections, the transfer correlations involving ammonia-water solution and lithium bromide-water systems are discussed, in which each one was classified by application (absorption or desorption) and geometry disposal. Additionally, these correlation are summarized in tables by application range and by test rig specifications. Next, others relevant falling film studies are showed, whose working fluid are different to the current study, but these have been used in ARC researches. Finally, the heat and mass transfer mapping of these correlations were carried out in a realistical operational conditions of an ARC for refrigeration ($-20°C$) and air-conditioning $7°C$ applications.

The study too aims compare the heat and mass transfer correlations, looking for a standard comparison for further studies, due that, currently, there are not a heat transfer correlation for ammonia-water falling film in absorption processes using nanoparticles [12].

2. Heat and mass transfer using falling films technology in sorption processes

The falling film technology can be used in different applications, such as in ARC. In this technology, there is a large heat transfer contact area between the wall surface and the liquid falling film, enhancing the heat removal for the absorption process case [2]. However, the whole heat and mass transfer resistance is concentrated in the thin liquid falling film [2, 13], and that transport process occurs within this film due to steady-state diffusion and heat and mass diffusion [13]. Fig. (2a) shows the general falling film technology on horizontal tubes and Fig. (2b) the temperature and concentration profiles for the absorptions process in a vertical plate. The generation process is used for evaporation or distillation processes, in which the wall temperature (T_w) is higher than the liquid falling film temperature (T_l), allowing the phase change (pure substance entering at the

saturated condition), or the separation process (no binary azeotrope substance entering at the saturated condition).

On the other hand, in the absorption process, the wall temperature (T_w) is lower than the liquid falling film (T_l), removing the heat of absorption ($\dot{Q}_{abs}$) and absorbing the vapor ($\dot{m}''_{abs}$) into the liquid falling film as shown in Fig. (2b), i.e., the heat of absorption is released at the liquid-vapor interface only, yielding an increase of the average film temperature (T_b), which diminishes the vapor solubility and, therefore, the absorption rate is strongly controlled by the intensity of heat removal from the liquid falling film to the coolant ($\dot{q}_c$) [2], while s and S are the inter-tube distances, respectively; T_c, T_{int} and T_v are the coolant, interface, and vapor temperature, respectively; x_b, x_{int} and y are the average concentration of the liquid falling film, the concentration of the liquid falling film at the interface, and the vapor concentration, respectively;

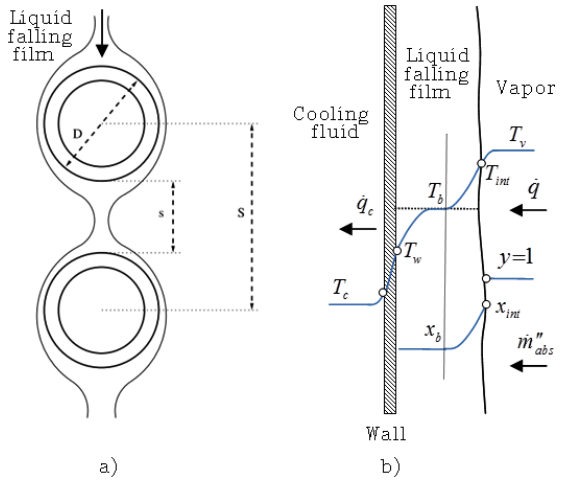

Figure 2: a) Falling film in horizontal tubes and b) temperature and concentration profiles for the ammonia-water absorptions process in a vertical plate (adapted from [2])

2.1. Heat and mass transfer coefficient calculation

In the falling film technology, the thermal resistance analogy is used to compute the global heat transfer coefficient between the bulk solution and the cooling or heating fluid, U, given by Eq. (1),

$$\frac{1}{U} = \frac{1}{h_l} + \frac{D_o}{2k_w} \ln \frac{D_i}{D_o} + \frac{D_i}{D_o h_{conv}} + f \tag{1}$$

where h_l is the heat transfer coefficient on the film, h_{conv} is the convective heat transfer coefficient associated to the secondary fluid, k_w the tube wall thermal conductivity, D_o, and D_i, the external and internal tube diameter, and f represents the fouling factor resistance ($0.0002 m^2\ ^\circ C\ W^{-1}$ [14] and [15] in ammonia-water pair, or $0.00009 m^2\ ^\circ C\ W^{-1}$ [16] in lithium bromide-water pair).

Heat and mass transfer coefficients cannot be directly evaluated from an experimental work. Therefore, they must be computed from measured quantities (e.g. temperature, concentration, liquid density) thanks to the Newton's law of cooling. This relation involves a difference in temperature, which takes into account, the wall temperature (T_w) and the interface temperature (T_{int}) in most of the cases. However, depending on how viscous sublayers are assumed both near the wall and near the liquid-vapor interface, two partial heat transfer coefficients can be defined (Fig. 2b) [2]:

- between the bulk liquid (T_b) and the wall (T_w):

$$h_{l,w} = \frac{\dot{q}_c}{T_b - T_w} \tag{2}$$

- between the liquid-vapor interface (T_{int}) and the bulk liquid (T_b):

$$h_{l,int} = \frac{\dot{m}''_{abs} \Delta i_{abs}}{T_{int} - T_b} \frac{1}{E_T} \tag{3}$$

where, E_T represents the Ackermmn's correction factor:

$$E_T = \frac{\Delta i_{abs}}{c_p} \frac{\ln(1 + c_p(T_{int} - T_b)/\Delta i_{abs})}{T_{int} - T_b} \tag{4}$$

in which, $\dot{q}_c$, $\dot{m}''_{abs}$ and i_{abs} represent the transferred heat to the cooling fluid, the absorbed mass flow rate per area and the absorption specific enthalpy, respectively; c_p is the specific heat at constant pressure.

Yüksel and Schlünder [2] employed $E_T \cong 1$. Nevertheless, this approximation stands for low values of heat flow through the liquid film, hence assuming a

linear profile for the temperature [13]. Thus, the average heat transfer coefficient reads:

$$\overline{h_l} = \frac{\dot{m}''_{abs}\Delta i_{abs}}{T_{int} - T_w} \tag{5}$$

The mass transfer coefficient (k_m) is defined by Eq. (6), while (ρ_l) and P represent the liquid density and the system pressure, respectively.

$$\overline{k_m} = \frac{\dot{m}''_{abs}}{\rho_l \ln(1 - x_b)/(1 - x_{int}(T_{int}, P))} \tag{6}$$

The use of the logarithmic mean difference is one of the most commonly used methods to compute the heat and mass transfer coefficient due to its simplicity [17]. However, Islam [18] and Fujita and Hihara [17] show that the logarithmic mean potential occurring in the average heat and mass transfer coefficient definition (Eqs. 7 and 8) presents wide deviations from experimental results. Due to that, the conventional method takes into account two separate processes of heat and mass transfer; the first one is the heat transfer from the liquid falling film to the cooling fluid, and the second is the absorption of refrigerant from the vapor phase to the cooling fluid, causing errors when there is not a non-linear temperature distribution of the liquid falling film in the absorber. However, the cooling fluid temperature distribution along the tube length is nearly linear [18]. Therefore, the logarithmic mean difference should be used only for low global heat transfer or under limited conditions [17].

$$\overline{h}_l = \frac{\dot{q}_c}{L\Delta T_{lm}} \tag{7}$$

and in the mass transfer coefficient definition:

$$\overline{k}_m = \frac{\dot{m}_{abs}}{L\Delta x_{lm}} \tag{8}$$

where, ΔT_{lm} and Δx_{lm} are the logarithmic mean temperature and concentration differences (Eqs. 9 and 10), respectively; $\dot{q}_c$, $\dot{m}_{abs}$, and L are the heat transferred from the liquid falling film to the cooling fluid, the absorbed mass of the vapor refrigerant into the liquid falling film, and the length of the absorber,

$$\Delta T_{lm} = \frac{(T_{l,i} - T_{c,o}) - (T_{l,o} - T_{c,i})}{\ln\left(\frac{T_{l,i} - T_{c,o}}{T_{l,o} - T_{c,i}}\right)} \tag{9}$$

$$\Delta x_{lm} = \frac{(x_{i,eq} - x_i) - (x_{o,eq} - x_o)}{\ln\left(\frac{x_{i,eq}-x_i}{x_{o,eq}-x_o}\right)} \tag{10}$$

where, T_l and T_c are the liquid falling film temperature and the cooling fluid temperature (both i-inlet and o-outlet), respectively; x_{eq} is the interfacial equilibrium concentration in T_l.

Another way to evaluate the heat or mass transfer coefficient is by employing a heat and mass transfer analogy, in which both transport mechanisms are considered merely diffusional through the liquid falling film (e.g. rectification process) and given by Eq. (11) [19], where M_m, Sc and Pr are the molecular weight, Schmidt number (0.6-2500) and the Prandtl number (0.6-2500), respectively.

$$\frac{h_l}{k_m} = c_p\ M_m\ \left(\frac{Sc}{Pr}\right)^{2/3} \tag{11}$$

Finally, for simultaneous heat and mass transfer processes, Treybal [20] proposed working with a corrected heat transfer coefficient ($h_l{}^*$), in which the effect of mass transfer on heat transfer were taken into account (Eqs. 12-13). Note that the effect of mass transfer on heat transfer can improve or deteriorate the heat transfer coefficient depending on both process directions, while $\dot{m}_i$ is the mass flow rate for the i^{th} component:A and B

$$h_l{}^* = h_l\ \frac{c}{1 - e^{-c}} \tag{12}$$

$$c = \frac{\dot{m_A} c_{p,A} + \dot{m_B} c_{p,B}}{h_l} \tag{13}$$

Thus, from an experimental work, the link between measured quantities and a relevant definition for transfer coefficients must be established carefully. Consequently, the resulting correlation has to be compared with other studies, as already done in many previous works (see Tab. 3 and Tab. 6)

2.2. Definition of dimensionless numbers, Nu, Sh and Re

Nusselt [21] analyzed the isothermal condensation phenomenon on a flat plate for a pure substance, assuming: laminar regime, Newtonian fluid, constant properties, and without inertial forces from the vapor acting at the interface, obtaining a correlation of the average heat transfer coefficient as a function of the acceleration of gravity, g, the Reynolds number, Re, and the fluid properties; dynamic viscosity, μ, density, ρ, and the liquid thermal conductivity k.

$$\frac{\overline{h}_l}{k}\left(\frac{\mu_l}{g\rho_l(\rho_l-\rho_v)}\right)^{1/3} = 1.467Re^{-1/3} \tag{14}$$

Neglecting the vapor density (ρ_v), and by the definition of kinematic viscosity ($\nu = \mu/\rho$), Eq. (15) yields,

$$Nu = \frac{\overline{h}_l}{k}\left(\frac{\nu_l^2}{g}\right)^{1/3} = \frac{\overline{h}_l L_c}{k} = 1.467Re^{-1/3} \tag{15}$$

in which, $L_c = (\nu^2/g)^{1/3}$ is known as the characteristic length or viscous length scale. However, the Nusselt number (Nu_δ) can be expressed (see e.g. [22, 23], as a function of the film thickness, δ, given by:

$$Nu_\delta = \frac{\overline{h}_l \delta}{k} \tag{16}$$

where δ may be used for the Nusselt film thickness, δ_{Nu}, in which, Γ represents the mass flow rate per unit length on each tube side, and θ the tube angle from the top or the wettability of the tube.

$$\delta_{Nu} = \left(\frac{3\mu\Gamma}{g\rho_l(\rho_l-\rho_v)\sin\theta}\right)^{1/3} \cong \left(\frac{3\nu\Gamma}{\rho_l g\sin\theta}\right)^{1/3} \tag{17}$$

Many correlations are based on Nu (Eq. 15), while others are based on Nu_δ (Eq. 16). In order to carry out a comparison between correlations, a common base must be established. Fortunately, both correlations are interchangeable and interconnected by the following correlation:

$$Nu_\delta = (0.75Re)^{1/3}\, Nu \tag{18}$$

In the same way, the Sherwood number, Sh, is defined as:

$$Sh = \frac{k_m}{D_m}\left(\frac{\nu^2}{g}\right)^{1/3} \tag{19}$$

and by

$$Sh_\delta = \frac{k_m \delta}{D_m} \tag{20}$$

Thus, the relations are linked by:

$$Sh_\delta = (0.75Re)^{1/3}\, Sh \tag{21}$$

Analogously, the Reynolds number involves the hydraulic diameter, D_h as the typical length:

$$Re = \frac{\rho V D_h}{\mu} = \frac{4\rho V \delta W}{\mu W} = \frac{4\dot{m}}{\mu W} = \frac{4\Gamma}{\mu} \tag{22}$$

or the typical length can be taken as the film thickness, δ (see e.g. [2, 24, 25])

$$Re_\delta = \frac{\rho V \delta}{\mu}\frac{W}{W} = \frac{\dot{m}}{\mu W} = \frac{\Gamma}{\mu} \tag{23}$$

Thus, the relation between these two correlations for the Reynolds number reads:

$$Re = 4Re_\delta \tag{24}$$

where, V represents the average fluid velocity, W the width or depth, $\dot{m}$ the mass flow rate. The ratio $\Gamma = \dot{m}/P_{wet}$ between the mass flow and the wet perimeter, is summarized in Table 1,

Table 1: Mass flow rate per unit length for various geometries

Γ, $[kgm^{-1}s^{-1}]$	**Geometry**
$\frac{\dot{m}}{2W}$	Horizontal tube or flat plate (both sides wet)
$\frac{\dot{m}}{W}$	Flat plate (one side wet)
$\frac{\dot{m}}{\pi D}$	Vertical tube

2.3. Classical hypothesis

In order to establish correlations for heat and mass transfer coefficient in sorption processes involving the falling film technology, standard hypotheses are assumed, such as steady-state, incompressible fluid, Newtonian fluid, thermodynamic equilibrium at the liquid-vapor interface, thermal physical properties are constant, non-condensable gases in mixture, and no chemical reactions. However, some additional specific assumptions are commonly encountered in the literature:

- Fluid flow assumptions
  - Laminar flow regime [2, 4, 14, 22, 23, 24, 25, 26, 27, 28, 29, 30, 31, 32, 33, 34, 35, 36, 37]
  - Turbulent flow regime [2]
  - No wave generation at the liquid-vapor interface or smooth falling film. (Waves -known as wavy laminar- improve the heat and mass transfer in the liquid falling film due the transport process. The capillary effects are significant in low Reynolds numbers ($Re \leq 200$), and the inertial effects are relevant in higher Reynolds number ($Re \geq 200$)[28]. However, a complete analysis of the simultaneous heat and mass transfer integrated to wave generation onto the interface is complex) [4, 22, 23, 34, 35, 36]
  - Wavy flow [28]
  - No interfacial shear or stagnated vapor at constant pressure [2, 4, 22, 23, 27, 30, 31]
  - Shear stress acting at the interface [14, 24]
  - Wall friction term is negligible [2, 24, 26]
  - Vapor and liquid flows are homogeneous [26]
  - No viscous dissipation (in low Reynolds number, this implies low flow velocities and, therefore, viscous dissipation can be neglected) [23, 28]

  - No pressure or velocity gradient in the main flow direction [4, 14, 23]
  - Transport governed by the convective-diffusion [28]
  - 2-D Model [28]

- Thermal transfer assumptions
  - No nucleate flow boiling regime [23, 34, 35, 36]
  - No heat transfer at the vapor phase [22, 23, 24, 27, 28, 30, 37]
  - Thermal resistance of tube wall is negligible [22, 23, 34, 35, 36]
  - Heat and mass transfer coefficients constants along the absorber tube [24, 26]
  - Vapor pressure driving equal to 0 at the inlet. No thermal entrance effects [2, 22, 23]. In contrast, Nakoryakov et al. [38] carried out an analysis of these effects in absorption/desorption processes, or Cerro and Whitaker [39] for general transport processes
  - Cross-streamwise diffusion. No diffusion in the flow direction [22, 23, 24, 28, 30, 34]
  - Wall temperature along the tube length changes in a linear fashion [23]
  - Constant wall tube temperature [25, 30]
  - No isothermal absorption [2], [24]
  - Saturation temperature in the inlet condition [30, 32, 28]
  - Subcooling temperature in the inlet condition [27, 32, 40]

3. Transfer correlations involving ammonia-water solution

ARC driven by ammonia-water pair can be used in applications of temperature ranging from subzero Celsius degree owing to the ammonia thermodynamic properties. Most studies on transfer correlations in literature focus on the absorber.

3.1. Absorber

The most frequent devices involving falling film are horizontal tubes, vertical plate surfaces and helical coil tubes.

3.1.1. Horizontal tubes

Bohra [31] carried out an experimental study on an ammonia-water ARC using the falling film technology, in which 24 tubes (4x6) of $0.0095m$ OD and $0.29m$ length were used. Flow patterns and the transport process were analyzed in his test bench, segmenting the absorber into six distinct parts. The lowest tubes of the array (where the cooling fluid enters in counter-current configuration) obtained higher ammonia absorption rates, similarly to Lee [37] and Lee [41]. In addition, the increase of the solution mass flow rate promoted an upgrade of the heat transfer coefficient because the liquid falling film reached a higher wettability on the tube wall. On the other hand, the heat transfer coefficient decreased as the absorber pressure (P_{abs}) and the weak solution concentration (x_{ws}) were also decreased.

The global heat transfer coefficient (U) ranged from 753 to 1853 $W\ m^{-2}\ ^{\circ}C^{-1}$, the film heat transfer coefficient ranged (h_l) from 923 to 2857 $W\ m^{-2}\ ^{\circ}C^{-1}$, the vapor mass transfer coefficient ($k_{m,v}$) ranged from 0.0026 to 0.25 $m\ s^{-1}$, and the liquid mass transfer coefficient ($k_{m,l}$) ranged from $5.51{\cdot}10^{-6}$ to $3.31{\cdot}10^{-5} m\ s^{-1}$. The following correlations represent the heat and mass transfer experimentally obtained by Bohra [31],

Nusselt number in the segmented liquid falling film, $Nu_{seg,\delta}$

$$Nu_{seg,\delta} = 7.589 \times 10^{-3} Re^{1.04} Pr^{0.45} \left(\frac{P_{abs}}{345}\right)^{-0.145} \tag{25}$$

Sherwood number in the segmented liquid falling film, $Sh_{seg,\delta}$

$$Sh_{seg,\delta} = 1.298 \times 10^{-4} Re^{0.57} Sc^{1.32} \left(\frac{P_{abs}}{345}\right)^{0.644} \tag{26}$$

Lee [37] studied the absorption process in the same test rig as Bohra [31], focusing on the analysis of the overall absorption process, in which both the vapor and the liquid phase correlations were obtained.

Nusselt number in the liquid falling film, Nu_δ

$$Nu_\delta = 3.22 \times 10^{-3} Re^{0.945} Pr^{0.743} \left(\frac{P_{abs}}{345}\right)^{-0.269} \tag{27}$$

Sherwood number in the vapor phase, Sh_v

$$Sh_v = 2.708 \times 10^{-11} \left(\frac{Gr_v Sc_v}{Ja_v}\right)^{1.256} \left(\frac{Pr_l}{Sc_l}\right)^{-1.681} \left(\frac{\mu_l - \mu_v}{\mu_v}\right)^{1.426} \tag{28}$$

while Gr and Ja are the Grashof number and the Jakob number, respectively.

Sherwood number in liquid falling film, Sh_δ

$$Sh_\delta = 7.437 \times 10^{-4} Re^{0.397} Sc^{1.04} \left(\frac{P_{abs}}{345}\right)^{0.8841} \tag{29}$$

where, P_{abs} is given in [kPa]. Next, Lee et al. [42] carried out an study focused to the absorption rates over horizontal falling film absorbers, using the same test rig and covering the influence of the operational effects over the heat and mass transfer rates. In addition, they compared their results with Wilke [43], Hu and Jacobi [44], Kwon and Jeong [14], and Meacham and Garimella [45]. Daguenet-Frick et al. [46] used this work to compare the heat transfer coefficient in water vapor absorption in aqueous sodium hydroxide process. However, the Reynolds number was not over the validation range [42]

3.1.2. Vertical surface

Kang et al. [27] carried out an experimental work on ammonia-water falling film absorption process using a vertical surface ($110 \times 130 \times 34\ mm^3$) with offset strip fins (OSF). The simultaneous heat and mass transfer coefficients were analyzed and computed for different operation conditions such as (a) inlet temperatures of the weak liquid solution ($T_{ws} = 17 - 37.2\ ^\circ C$) and the ammonia vapor ($T_v = 54.5 - 66.5\ ^\circ C$), (b) mass flow rate of weak liquid solution ($\dot{m}_{ws} = 0.004 - 0.01015 kg\ s^{-1}$) and the ammonia vapor ($\dot{m}_v = 0.00062 - 0.00090 kg\ s^{-1}$),

and (c) weak liquid solution concentration ($x_{ws} = 5, 10$, and 15 %). The absorber used water as secondary cooling circuit ($\dot{m}_c = 0.0647 - 0.0797 kg\ s^{-1}$), circulating in a counter flow configuration to the liquid falling film. A rectification process of the wet ammonia vapor was reached before being absorbed by the liquid falling film in the absorption process due to the deeply low level of ammonia vapor purity ($y = 64.7 - 79.7\%$) and to the inlet subcooling conditions.

The heat and mass transfer ranged from 500 to $2100 W\ m^{-2}\ ^{\circ}C^{-1}$ and from 1.0 to $55 \times 10^{-5} m\ s^{-1}$, respectively. The increase of the falling film Reynolds number and the mass flow rate of ammonia vapor enhanced the Nusselt and the Sherwood number. However, the Nusselt number was more affected by the liquid mass flow rate than the mass flow of ammonia vapor, while the Sherwood number was more affected by the Reynolds number of ammonia vapor than the Reynolds number of liquid solution. On the other hand, the Sherwood number values were higher than the Nusselt number owing to the Lewis number, meaning that the effective thickness of thermal boundary layer is thicker than that of the diffusion boundary layer [27]. The following Nusselt and Sherwood number correlations were obtained,

Nusselt number in the liquid falling film, Nu

$$Nu = 8.530 \times 10^{-2} Re_l^{1.518} Re_v^{0.1759} \left(\frac{T_v - T_l}{T_l} \right)_i^{1.8790} \left(\frac{x_v - x_l}{x_l} \right)_i^{-0.5756} \quad (30)$$

Sherwood number in the liquid falling film, Sh

$$Sh = 6.996 \times 10^{-6} Re_l^{0.8874} Re_v^{1.265} \left(\frac{T_v - T_l}{T_l} \right)_i^{0.8844} \left(\frac{x_v - x_l}{x_l} \right)_i^{0.5304} \quad (31)$$

Lee et al. [47] compared the performance of falling film and bubble absorbers for the same operation conditions. Bubble absorbers reached a better performance than falling film for low liquid Reynolds numbers and high vapor Reynolds numbers because there was a partial wettability of the tube in the falling film technology [4]. However, the bubble mode may transfer less heat to the cooling fluid than the falling film for a high liquid solution and low ammonia vapor, resulting in a higher heat generation than of the falling film.

Nusselt number in the liquid falling film, Nu

$$Nu = 0.01369 Re_l^{0.5103} Re_v^{0.02461} \left(\frac{T_v - T_l}{T_l} \right)_i^{0.2977} \left(\frac{x_v - x_l}{x_l} \right)_i^{0.1438} \quad (32)$$

Sherwood number in the liquid falling film, Sh

$$Sh = 658.46 Re_l^{0.0195} Re_v^{0.9571} \left(\frac{x_v - x_l}{x_l} \right)_i^{-0.0639} \quad (33)$$

3.1.3. Helical coil

The helical geometry may be an alternative to obtain a more compact machine because the heat transfer area per unit volume increases. Jeong et al. [15] experimentally investigated the performance of the heat transfer coefficient without mass transport in a coiled tube absorber for various operation conditions such as (a) solution flow rate ($\dot{m}_{ws}$), which was up to $0.06 kg\ s^{-1}$, (b) ammonia vapor ($\dot{m}_v$) ranged from 0.00009 to 0.00042 $kg\ s^{-1}$, and (c) inlet concentration (x_l) between 1.2 to 2.2 %. The tests were carried out with and without the ammonia absorption process, using a counter-flow absorption in which density (ρ_l), temperature (T), and pressure (P) were used to find the ammonia concentration.

The heat transfer coefficient (h_l) was enhanced when the solution flow rate ($\dot{m}_l$) increased (for both with and without absorption process). However, the heat transfer coefficient (h_l) associated with the absorption process was lower than the heat transfer obtained for pure water at the same mass flow rate because the ammonia vapor feeding in a counter-flow to the falling film caused an uneven distribution or a stagnation of the liquid falling film [15]. Nevertheless, the mass transfer (k_m) behavior was not studied on the test rig. Finally, the Nusselt number as a function only of the Reynolds number was proposed for ammonia-water

$$Nu = 0.00022 Re \quad 50 \leq Re \leq 300 \quad (34)$$

Kwon and Jeong [14] experimentally analyzed the effect of the vapor flow direction over the heat transfer coefficient (h_l) for the absorption process at three different concentrations (3, 14, and 30 %) in a helical coil configuration.

The effect of the mass flow rate ($\dot{m}_l$) and the temperature of the weak liquid solution (T_{ws}) were investigated in the laminar regime (Re=10-250). A $0.6m$ tube length and $0.0127m$ OD was manufactured as a helical coil heat exchanger at $0.0827m$ and $0.08m$ of an average diameter of a coil (#30) and the header height, respectively. For the balance equations of the absorption process, the heat transferred from the absorber to the cooling fluid circuit was expressed for both absorption processes (heat latent transfer) and change in the solution temperature (sensible heat transfer). The effects of vapor flow over the heat transfer coefficient (h_l) were prominent when there was a counter-flow absorption and a low ammonia concentration (3%) because, in small concentrations, the vapor has high specific volume. Moreover, the liquid falling film flow pattern may be affected by a high velocity of the vapor flow. The Nusselt number was higher in the co-current absorption than in the counter-flow absorption. However, at a higher ammonia concentration (30%), the behavior of the Nusselt number was similar for both co-current and counter-flow absorption processes. In addition, the increase in the liquid solution mass flow rate improved the heat transfer coefficient. On the other hand, the effect of the weak liquid solution temperature over the heat transfer was negligible when it was compared with other operational parameters.

The Nusselt number for the liquid falling film for co-current absorption is given by Eq. (35), where τ_v^* is a non-dimensional shear stress detailed by Kwon and Jeong [14].

$$Nu = 1.975 \times 10^{-3} Re_l^{0.6895} \tau_v^{*-0.0249} \tag{35}$$

Nusselt number in the liquid falling film for counter-current absorption

$$Nu = 1.683 \times 10^{-4} Re_l^{0.8672} \tau_v^{*-0.3018} \tag{36}$$

3.2. Generator using horizontal tubes

Zavaleta and Simões-Moreira [36] analyzed a falling film generator (distiller) to optimize the concentration (y) and the mass flow rate of distilled ($\dot{m}_y$) when

the ammonia vapor is separated from the ammonia-water solution, researching some mean parameters such as strong solution concentration (x_{ss}), strong solution mass flow rate($\dot{m}_{ss}$), rectifier temperature (T_{rect}), wall temperature (T_w) and strong solution temperature of inlet (T_{ss}). A horizontal tube bundle geometry was used as a generator and rectifier, analyzing the hydraulic behavior of the liquid film and the distillation degree of purity. In the first one, a total wettability on the tubes was reached due to the small intertube distance, ($S - D = 2\ mm$), homogeneous liquid distribution, and a superficial treatment by sand blasting over the wall tube.

A distilled ammonia concentration (y) up to 99.74% was obtained for an ammonia-water concentration of $x_{ss} = 49\%$. In addition, the purity of distilled ammonia (y) was enhanced when the strong solution mass flow ($\dot{m}_{ss}$) and the strong solution concentration (x_{ss}) were increased, or when the average rectifier temperature (T_{rect}), wall temperature (T_w) in the generator, and the strong solution temperature (T_{ss}) were reduced. The experimental work was carried out for a strong solution mass flow of 0.0160 to 0.0276 $kg\ s^{-1}$ equivalent to Reynolds numbers of 108 to 246. They employed two ammonia concentrations (0.37 and 0.49). The concentration of ammonia distilled (y) was increased, and the distilled mass flow rate ($\dot{m}_y$) was diminished with the increase of the mass flow rate ($\dot{m}_{ss}$) when the wall temperature and the rectifier temperature were kept constant, because the heat transfer coefficient diminishes due to the thickening of the liquid film, increasing the thermal resistance throughout the liquid film. According to the rectifier temperature, higher ammonia distilled concentration was obtained at the cooler temperatures since it rejected more water of the wet ammonia vapor [36].

Regarding the wall temperature (T_w), the distilled mass flow ($\dot{m}_y$) improved for the highest wall temperature (T_w) in the generator, however, the distilled concentration diminished (y), because a higher wall temperature promoted the evaporation of more wet vapor [36]. The following correlation was derived for

the heat transfer on the liquid film:

$$Nu = 0.75 Re^{-0.27} Pr^{0.4} \tag{37}$$

3.3. Summary of transfer correlations

In this section, the correlations presented previously are summarized: in Tab. 2, the application range of the correlations related to ammonia-water solution is summarized. Most of the correlations are devoted to the absorption machine. To our knowledge, there exists only one work in the literature proposing a correlation for a generator using ammonia-water solution. The first and second columns shows the author and the equation correlations, respectively; Next, Prandtl, Reynolds and Schmidt numbers are showed; while temperature and pressure of aplication are showed in the next two columns; finally, the two last columns present the concentration of the liquid solution (x) and the vapor (y), and the remarks for each correlation. Finally, in Tab. 3, the configurations of the experimental set up are summarized. The first column present the author, the second column show the geometrical specifications; next column associates other studies that they have been used to being compared; finally, some comments was carried out in the last column

Table 2: Application range of the correlations

Author	Correlation	Pr	Re	Sc	T,°C	P,kPa	x, % y, %	Remarks
Falling film Absorber using Ammonia-Water solution								
Bohra [31]	25, 26	2.2-10.4 $0.5-0.93$	$26-157$ -	$45.4-588.1$ $0.5-0.53$	$14.8-105.4$ $(-10.5)-28.2$	$169-520$	$5;15;25;40$ -	
Jeong [15]	34	$2.4-3.9$ -	$20-300$ -	-	$45-54$ $66-69$	$67-117$	$1.2;3.7$ $63;77$	
Kang [27]	30, 31	$3.8-5.8$ -	$17-24$ -	$33.8-39.2$ -	$17.0-37.2$ $54.5-66.5$	101.3	$5;10;15$ $64.7-79.7$	
Kwon [14]	35, 36	$2.1-3.8$ -	$10-250$ -	-	$45-60$ -	$17-193$	$3;14;30$ $45.6;84.4;96.5$	
Lee [37]	27, 28, 29	$2.2-8.2$ $0.5-0.93$	$29.7-169.2$ -	$43.6-362.7$ $0.5-0.53$	$14.8-105.4$ $(-10.5)-28.2$	$169-520$	$5;15;25;40$ -	$Gr_v = 4223-59893$ $Ja_v = 0.0098-0.0387$
Lee [47]	32, 33	$3.8-5.8$ –	$50-700$ $25-200$		$15.5-20$ –	101.3	$0.1-0.3$ –	
Other works using Ammonia-Water solution								
Zavaleta [36]	37	$1.68-2.65$	$108-246$	-	$87-103$	$1460-1611$	$37;49$	Generator

4. Transfer correlations involving lithium bromide-water solution

The sorption machine using lithium bromide solution works both at *low* pressure (around 1 kPa) where the $Li-Br$ solution absorbers the water vapor, and at *high* pressure (around 10 kPa) where the desorption process occurs. Although the absorber constitutes the critical device in the machine, many studies have also focused on the generator.

4.1. Generator

The main devices used for generators involving lithium-bromide pair are vertical tubes and horizontal tubes.

4.1.1. Vertical tubes

Shi et al. [34] carried out a mathematical simulation and experimental work of a desorption process inside a vertical tube of $25mm$ OD and $760mm$ in length, analyzing the influence of the heat flux and the volume flow rate over the heat transfer coefficient for a single absorption pressure ($97.25kPa$), solution concentration of 49.5%, heat flux ranging $5-25kW\ m^{-2}$, and for Reynolds smaller than 500 [1]. In the mathematical analysis, the interfacial effects, wave generation

[1] Reynolds number was defined as a function of the film thickness, Re_δ

Table 3: Summary of configuration studies on absorption and generation using ammonia water

Experimental works using Ammonia Water: Configuration of study			
Author	**Geometrical specifications**	**Compared**	**Comments**
Bohra [31]	Horizontal tube bundle $4Cx6R$ $O.D = 0.0095m$, $L = 0.29m$, $S = 0.0201m$ $\delta_w = 0.0007m$ $A_{total} = 0.210m^2$	Wilke [43], Dorokhov [48], Hu and Jacobi [49] Kwon [14], Meacham [50], Meacham [51]	Water counter-current cooling and Counter-current absorption
Jeong [15]	Coiled tube $O.D = 0.0127mm, I.D = 0.0107mm$ $\overline{Dcoil} = 0.0827m$		Water co-current cooling and Counter-current absorption
Kang [27]	Surfaces as offset strip fin stainless steel $0.1 * 0.13 * 0.034mm^3$ Fin pitch $= 1.95mm$, $\delta_w = 0.0002m$ Fin height $= 0.0048mm$ $A_{total} = 0.0143m^2$		Water counter-cross cooling and Co-current absorption
Kwon [14]	Coiled tube $O.D = 0.0127mm, I.D = 0.0107mm$, $L = 0.6m$ $A_{total} = 0.024m^2$		Water co-current cooling and Co/counter-current absorption It took into account the shear stress at the vapor-liquid interface It used the same test rig as Jeong [15]
Lee [41]	Three surface types smooth plate, hair lined plated treated by laser, and plate treated by sand paper (higher wettability) $0.112 \times 0.264 \times 0.0003m^3$, and $A_{total} = 0.0296m^2$		Bubble, Water counter-current cooling Counter-current absorption
Lee [47]	Three surface types smooth plate, hair lined plated treated by laser, and plate treated by sand paper (higher wettability) $0.112 \times 0.264 \times 0.0003\,m^3$, and $A_{total} = 0.0296\,m^2$	Lee [47]: bubble tecnology	Bubble Water counter-current cooling Counter-current absorption
Zavaleta [36]	Horizontal stainless steel tube bundle 7 Col x10Row $\delta_w = 0.001m$, $O.D = 0.008m$, $L = 0.15m$ $A_T = 0.264m^2$	Hu and Jacobi [49], Wilke [43],Chun and Seban [52] Mitrovic [53], Owens [54], Fujita [55]	Generator-Rectifier Heating by thermal oil-Generator Water cooling-Rectifier Ammonia water. A 100% surface wettability was achieved for Re above 100 up to nearly 250 Properties by EES and Conde [56]

in the liquid film, changes in film thickness, and pool boiling by superheating (only by the evaporation on the interface) were neglected. In addition, the performance of the flooded generator and the falling film evaporator were compared for the same heat flux.

The heat transfer coefficient $(1000 - 1800W\ m^{-2}\ ^{\circ}C^{-1})$ was enhanced when the heat flux was increased for different volume flow solutions. However, the heat transfer rate decreased with the increases of the volume flow solution when the Reynolds number was less than $Re_\delta \leq 500$ or $Re \leq 2000$, and for $Re_\delta \geq 500$. The heat transfer behavior was the opposite when the volume flow was

incremented because there was a regime transition from the laminar to the turbulent regime.

According to the numerical and experimental analysis, both results of the heat transfer coefficient were compared, having the heat transfer coefficient underestimated by the numerical study due to the simplified hypotheses previously mentioned. Finally, the falling film evaporator had the best performance of the heat transfer coefficient for heat flux lower than $12.000W\ m^{-2}$ as compared with the flooded generator.

Heat transfer coefficient ($\pm 19\%$ maximum deviation) for the liquid-phase

$$h_l = 14009.87 {q''_w}^{0.0764} Re_l^{-0.5391} \tag{38}$$

Later, Shi et al. [35] built a test rig to investigate the heat transfer behavior for a vertical in-tube falling film generator, testing different heat fluxes ($10 - 25kW\ m^{-2}$) and concentrations of lithium bromide ($49.5 - 58\%$) for a laminar regime ($Re = 287 - 770$), and for other operation conditions such as (a) generation pressure of $9.725kPa$ and (b) volume flow rate range of $7 - 14ml\ s^{-1}$. A $25mm\ O.D$ stainless steel tube and $760mm$ length was employed, in which the lithium bromide solution was fed inside the tube top in the saturated condition. In addition, the falling film technology was compared with the flooded generator as well.

According to the inlet concentration of lithium bromide solution, the change in this parameter promoted the variation in the thermophysical properties, meaning the increases of the viscosity and the surface tension when the concentration was increased, diminishing the inertial flow effects, and thus, the convection heat transfer decrease on the solution side. On the other hand, the increase of the heat flux may have modified the heat transfer mechanism from the evaporation process given at the interface to the evaporation process accompanied by nucleate boiling, which implied increase of the heat transfer coefficient, as usual. However, Shi et al. [35] did not study these phenomena in an independent fashion. Finally, the heat transfer coefficient in the falling

film technology reached higher performance (up to 4 times) than flooded tube generator, making the design of a desorption equipment more compact.

Heat transfer coefficient for the liquid-phase

$$h_l = 129.7712{x_i}^{-0.8058} q_w^{0,2422} Re_l^{-0.0856} \tag{39}$$

where, x_i is the weak solution concentration at the inlet condition and q_w is the heat transferred by the wall.

4.1.2. Horizontal tubes

Jani et al. [30] developed a model to analytically study the heat and mass transfer coefficient in a falling film generator over a horizontal tube bundle, in which the Reynolds numbers (in the laminar regime without wave generation), tube diameter, tube spacing, and thermophysical properties were analyzed. The model took into account three regions over the horizontal tubes for different heat and mass transfer phenomena, being (a) impingement region on the top of the tubes, (b) vertical liquid sheet for the tube spacing, and (c) tube bundle for all horizontal tubes. Prandtl numbers ranged from 7 to 10, Reynolds number ranged from 100 to 500, generation pressure from 5 to $10kPa$, and lithium bromide concentration from 50 to 60%.

The average heat transfer coefficient decreased with the increase of the number of tubes in the vertical position in the bundle tube, being expressed as a function of the tube numbers (N) and the heat transfer coefficient (h) of the first tube, $hN^{-0.25}$. For low Reynolds numbers ($Re \leq 200$), the increase in the Reynolds number improved the average heat transfer rate. However, above this value, the effects of the Reynolds number over the average heat transfer coefficient may be neglected as well as the generation pressure variations or the superheating wall.

Nusselt number for the liquid phase for one tube

$$Nu = 0.5441 Re_l^{0.1597} Pr_l^{0.4563} {D^*}^{-0.3971} {s^*}^{0.001626} P^{0.0213} e^{-0.004598X} \tag{40}$$

Nusselt number for bundle tube

$$Nu = 0.5441 Re_l^{0.1597} Pr_l^{0.4563} D^{*-0.3971} s^{*0.001626} P^{0.0213} e^{-0.004598X} \cdot N^{-0.25} \tag{41}$$

where D^* and s^* represent the dimensionless tube diameter (D/L_c) and the dimensionless vertical tube spacing (s/L_c), respectively. L_c represents the characteristic length $(\nu^2/g)^{1/3}$.

Jani [57] proposed correlations for the dimensionless heat and mass transfer coefficients obtained by numerical modelization. The configuration studied corresponds to a solution of $Li - Br$ falling down over a horizontal single heated tube.

The model used for the hydrodynamic part corresponds to the Nusselt solution (the stream-wise component of velocity is quadratic for a given cross section of the liquid film) but varied following the angle along the tube. The transport equations correspond to the steady advection-diffusion equations.

An increase of absorption pressure led to an increment of the saturation temperature of the solution, reducing the viscosity of solution, and therefore, an enhancement of the heat and mass transfer coefficient. On the other hand, the viscosity could be increased with a higher inlet concentration, negatively affecting the equipment performance [57]. The correlations obtained were

Nusselt number for the liquid phase

$$Nu = 0.7893 \times Re_l^{0.16587} Pr_l^{0.37275} Sc_l^{-0.041769} D^{*-0.40335} \tag{42}$$

Sherwood number for the liquid phase

$$Sh = 0.002 \times Re_l^{1.0023} Pr_l^{-0.74049} Sc_l^{1.3455} D^{*-1.0006} \tag{43}$$

where D^* represents the dimensionless diameter of the tube as previously defined. The range of validity holds for values of Pr between 7 and 10, values of Re between 100 and 500. The pressure values from $5kPa$ to $10kPa$ and the concentration of lithium bromide used was around 50% to 60%

According to the results, the Nu number increased as the Re_l number also

increased, but seemed to be unaffected by the Sc_l number. The Sh number grew linearly with the Re_l number but remained proportionally inverse to the tube diameter. An increase of the generator pressure (or saturation temperature) and/or a reduction of the inlet concentration improved the heat transfer coefficient due to the thinning of the falling film by a decrease of the viscosity.

4.2. Absorber

Most of the works devoted to absorbers using lithium bromide-water solution are focused on vertical flat plate and horizontal tubes.

4.2.1. Flat plate

Kim and Ferreira [32] studied the heat and mass transfer coefficients enhancement, for vertical plate absorber, thanks to the presence of wire screen, when the Re_l number is varying (from 40 to 110). In their investigation, four different liquid films are used: pure water and a 50% $\mathrm{Li-Br}$ solution, with or without 100 *ppm* of 2-ethyl-1-hexanol (2-EH) as additive. The experimental setup uses a flat copper plate that may be covered by a wire screen. For the whole 39 data set obtained, the range used for pressure was from 0.7 to $2.9kPa$. The mass flow rate at the inlet varied from 0.6×10^{-3} to $7.7 \times 10^{-3} kg\ s^{-1}$. The resulting correlations are given by

Nusselt number for the liquid phase

$$Nu = a \times Re_l^b Pr_l^{0.5} \tag{44}$$

Sherwood number for the liquid phase

$$Sh = c \times Re_l^d Sc_l^{0.5} \tag{45}$$

where, for 4 configurations (over the 10 performed), the coefficients are presented in Table 4.

The global result shows that the presence of the wire screen tends to decrease both heat and mass transfer coefficients of $\mathrm{Li-Br}$ solution when mixed with

Table 4: Constant for equations (44) and (45)

Configuration	a	b	c	d
Solution, Bare	0.0249	0.069	0.896	-0.3
Solution, Screen	0.00493	0.469	0.965	-0.343
Solution + 2-EH, Bare	0.0259	0.247	2.623	-0.265
Solution + 2-EH, Screen	0.0166	0.279	0.886	-0.24

the 2-EH additive. Specifically, for the heat transfer coefficient, the screened surface slightly enhances transfers by promoting the wetting surface of pure $Li - Br$ solution, in comparison with the bare surface. Yet the reciprocal occurs when 2-EH is added: the screen tends to reduce the heat transfer. For the mass transfer, the Sh number remains higher when the solution is water-cooled than for the adiabatic case. In the former configuration, the presence of the wire screen tends to weaken the mass diffusion when the 2-EH additive is used. The wire screen produces the converse effect (increasing the mass diffusion) for solutions without additive. The presence of the wire screen seems not to produce any significant effect on the Sh number for other configurations.
However, the authors highlight that their analysis does not take into account incomplete wetting. Moreover, an error analysis yielding a possible error to heat transfer coefficient estimation of $\pm 20\%$, in case of water-cooled absorption.

Karami and Farhanieh [22] carried out a numerical study of the simultaneous heat and mass transfer phenomenon in the absorption process in a vertical plate using the lithium bromide-water as the working fluid, analyzing (a) the effects of the solution mass flow ($Re = 5 - 150$), (b) inlet cooling temperature, and (c) the inlet solution concentration. A fully implicit finite-difference method was used to solve the one-dimensional mass, energy and momentum equations, analyzing the grid size effects and then employed the 800×160 mesh, and the mass flux value as convergence criteria (10^{-6}).

The temperature distribution across the film thickness was assumed to be linear due to the dominating heat only conduction effect, in which the lowest temperature profile was obtained in the last section of the absorber. The mass transfer rate reached a maximum value of $5.1799 \times 10^{-3} kg\ m^{-2} s$. The local heat transfer coefficient changed as a function of the vertical position on the plate (up to 5 times). Nevertheless, the local mass transfer coefficient was strongly dependent on the vertical position (up to 12 times), having the highest values in the first section of the absorber [22]. The correlations based on the numerical results were,

Nusselt number for the liquid phase

$$Nu_{\delta} = 0.4767 Re_l^{0.0477} Pr_l^{0.334} \tag{46}$$

Sherwood number for the liquid phase

$$Sh_{\delta} = 0.1329 Re_l^{1.0571} Sc_l^{0.334} \tag{47}$$

Later, Karami and Farhanieh [23] carried out the similar numerical modeling to analyze the simultaneous heat and mass transfer behavior for different inclinations of the flat plate, covering from the quasi-horizontal position ($\beta = 10°$) up to the vertical position ($\beta = 90°$). The absorption mechanism occurring within the film was modeled by the 2D steady advection-diffusion equations, tested for the absorption pressure of $P = 1kPa$, inlet solution temperature fixed at $45°C$, whereas the inlet concentration was 60%. The properties of the lithium bromide-water solution were taken from McNeely [58].The Reynolds number ranged from 4 up to 150 for different flat plate inclinations, β, proposing the following correlations,

Nusselt heat transfer for the liquid phase

$$Nu_{\delta} = A \cdot Re_l^B Pr_l^{0.334} \tag{48}$$

Sherwood number for the liquid phase

$$Sh_{\delta} = C \cdot Re_l^D Sc_l^{0.334} \tag{49}$$

with coefficients A, B, C and D depending on the angle and given by equations (50) to (53).

$$A = 6 \times 10^{-8}\beta^3 - 2 \times 10^{-5}\beta^2 + 1.4 \times 10^{-3}\beta + 1.58 \times 10^{-2} \quad (50)$$

$$B = -1 \times 10^{-7}\beta^3 + 3 \times 10^{-5}\beta^2 - 3 \times 10^{-3}\beta + 5.637 \times 10^{-1} \quad (51)$$

$$C = -2 \times 10^{-7}\beta^3 + 3 \times 10^{-5}\beta^2 - 2.3 \times 10^{-3}\beta + 1.31 \times 10^{-1} \quad (52)$$

$$D = 3.23 \times 10^{-6}\beta^2 - 6.19 \times 10^{-4}\beta + 1.16 \quad (53)$$

Following their results, the averaged Nu does not seem to be highly affected (variations inferior to 0.07) for different inclination at $Re_l = 20.5$, whereas the averaged Sh number reduces by about 42% (from 46 to 27) when the angle goes from 10° to 90°. Moreover, the formulas performed shows that the optimal angle for the averaged Nu seems to be for an inclination around $\beta = 85°$.

4.2.2. Horizontal tubes

Babadi and Farhanieh [59] developed an analytical study of the heat and mass transfer phenomena in the lithium bromide-water absorption process over a horizontal tube for operation conditions such as (a) Reynolds number ranging from 5 to 100, (b) absorption pressure of $1kPa$, (c) inlet concentration of 62%, (d) wall temperature of $32°C$, and (e) inlet temperature of $40°C$. The average heat transfer coefficient ranged between 2000 and 5000 $W\ m^{-2}\ °C^{-1}$.

A large temperature difference between the tube wall and the inlet solution promoted the highest value of heat transfer rate. In contrast, at the outlet region, the heat transfer decreased due to the thickening of the liquid film, increasing the thermal resistance. Moreover, the film thickness was associated with the Reynolds number changes, meaning the diminishing of the heat transfer rate with the decreasing of the Reynolds number due to the viscosity effects were more prominent than the inertial effects. In the opposite behavior, a high Reynolds number promoted convective heat transfer rate. Nevertheless, the Reynolds number influence was more dominant over the mass transfer than over the heat transfer rate [59]. Banasiak and Kozioł [60] used this study to compute the heat transfer coefficient

Nusselt number for the liquid phase

$$Nu = 0.45 Re_l^{-0,23} Pr_l^{0.33} \qquad \text{for} \qquad Re < 60 \tag{54}$$

Sherwood number for the liquid phase

$$Sh = 1.03 Re_l^{-0.146} \left(\frac{Sc_l}{1000} \right)^{1.42} \qquad \text{for} \qquad Re < \left(\frac{Sc_l}{5367} \right)^{-3.61} \tag{55}$$

$$Sh = 0.094 Re_l^{0.29} \left(\frac{Sc_l}{1000} \right)^{2.6} \qquad \text{for} \qquad Re > \left(\frac{Sc_l}{5367} \right)^{-3.61} \tag{56}$$

4.3. Summary of transfer correlations

Table 5: Application range of the correlations

Author	**Correlation**	***Pr***	***Re***	***T*,°C**	***P*,*kPa***	***x***	**Remarks**
Generator falling film using Lithium bromide-water solution							
Jani [30]	40, 41	$7-10$	$100-500$	$60-140$	$5-10$	$50-60$	
Jani [57]	42, 43	$7-10$	$100-500$	$60-140$	$5-10$	$50-60$	$Sc = 268$
Shi [34]	38	$3.8-4.7$	$\leq 500^*$	$126-150$	97.25	$49.5-58$	$q'' = 5-25 kW/m^2$
Shi [35]	39	$5.6-10.61$	$287-770$	$126-150$	9.725	$49.5-58$	$q'' = 10-25 kW/m^2$
Absorber falling film using Lithium bromide-water solution							
Babadi [59]	54, 55, 56	28.5	$5-100$	40	1	62	
Karami [22]	46, 47	17.7	$5-150$	45	1	60	
Karami [23]	48, 49	17.7	$5-150$	45	1	60	Inclined plate
Kim [32]	44, 45	$\cong 11-15$	$40-110$	$18-42$	$0.7-2.9$	50	

Table 6: Summary of configuration studies on sorption process using lithium bromide

Author	Geometrical specifications	Compared	Comments
Analytical and Numerical works using Lithium Bromide: Configuration of study			
Babadi [59]	Horizontal tube $D = 20mm$		Method: finite difference method. Assumes the total wettability of the tube
Jani [30]	Tube bundle $D = 19.05mm, S = 0.03m$	Kim [61], Jani [62]	Method: Non-linear differential equations solved by Runge-Kutta. The position tube effect on the row tube bundle is analyzed
Jani [57]	Horizontal tube $D = 19.05mm$	Kim [61], Shi [35], Nusselt [21]	Method: implicit Crank-Nicolson method
Karami [22]	Vertical plate $L = 1m$	Medrano [63]	Method: Fully implicit finite difference. Properties: Florides [16], and McNeely [58]. Convergence criterion: mass flux (10^{-6})
Karami [23]	Incline plate $L = 1m$	Medrano [63]	Properties: Florides [16], and McNeely [58]. Method: Implicit finite difference. Convergence criterion: mass flux (10^{-6})
Experimental works using Lithium Bromide: Configuration of study			
Kim [32]	Flat plate-smooth copper surface and copper+wire screen Screen: woven with $0.38mm$ copper wire, having 22 meshes per inch. $0.095x0.540m$ $A_{total} = 0.0513m^2$	Heat transfer: Hoffmann [64] Mass transfer: Yih [65] Nagaoka [66], Kim [67]	Adiabatic condition are tested too. Properties: thermodynamic properties of [68] k, μ of [69], and D_m of [70]
Shi [34]	Vertical tube $L = 0.760m$, $O.D = 0.025m$		Study with modelization
Shi [35]	Vertical stainless steel in−tube $\delta_w = 0.002m$, $O.D = 0.025m$, $L = 0.76m$		Overall heat transfer in-tube falling film is 4.37 times higher than immersed generator

5. Other works devoted to transfer coefficient study

Some other works focus on establishing a formula for heat transfer coefficient. These works may involve the specific geometric length (whose influence has been suggested in the previous graphs), or the study is simply dedicated to fluid couples other than ammonia-water or lithium bromide-water.

5.1. Works using lithium bromide-water couple

Yüksel and Schlünder [2] carried out an experimental study of a non isothermal absorption in liquid films for the laminar and turbulent regime, in which the local and the average heat and mass transfer coefficients were analyzed. A vertical tube with variable length $(0 - 2.5m)$ and the counter-current absorption was configured. There was not any mass transfer resistance in the vapor phase and the film surface temperature was measured by infra-red pyrometer $(\pm 0.3K)$.Two partial heat transfer coefficients were defined, being (a) from the film surface to the bulk, and (b) from the bulk to the vapor-liquid interface. For the former, the wall temperature and the bulk temperature were taken into account, and for the second, the bulk temperature and the interface were taken into account (Eqs. 2 and 3). The average heat and mass transfer were given by,

$$\bar{h_l} = \frac{\dot{m}''_{abs}\Delta i_{abs}}{T_{int} - T_w} \tag{57}$$

$$\bar{k_m} = \frac{\dot{m}''_{abs}}{\pi D \bar{\rho_l} \int_0^L ln(\frac{1-x_b(L))}{1-x_{int}(L)})} \tag{58}$$

For the turbulent regime, it was assumed that the interface temperature has the same value as the bulk temperature, and the turbulence is damped in the vicinity of the vapor-liquid interface due to surface tension effects; thus, at the interface, the heat, mass and momentum transfer were only possible by molecular transfer, making possible to use an analogy between the temperature and concentration profile (Nu/Sh) as follows [2];

$$(\frac{1 - x_b}{1 - x_{int}(T_{int}, P)})^{\frac{\frac{c_{p,water}}{c_{p,l}}}{Le^{1-n}}} = \frac{c_{p,water}}{\Delta i_{abs}} T_{int} - T_b + 1 \tag{59}$$

The n values are between 0.4 to 0.5 for isothermal falling film absorption. They found that assuming the same value for the bulk and the interface temperatures led to low Sherwood numbers. However, their results of mass transfer obtained by interface temperature measurements agreed well with the calculated by Nu/Sh analogy. In addition, for the Reynolds number in the $100-500$ range, the mass transfer is highly sensitive to the vapor phase velocity because it amplified the shear stress over the interface. The turbulent regime is less dependent on this condition because the mass transport is severe in the turbulence [2]. According to the Nusselt number, the Nu/Sh analogy agrees with that computed by interface temperature measurements, but when it take into account the assumption of the same temperature between bulk and interface, it overestimates the Nusselt number.

Yüksel and Schlünder [24] carried out a mathematical modeling of turbulent heat and mass transfer in a non-isothermal falling film absorption, in which the mean assumptions were taken into account: (a) the transversal velocity does not influence the momentum transfer, (b) no axial diffusive transport process, (c) no pressure gradients into the film, (d) shear stress acting on a differential element of the film, (e) film thickness computed by continuity equation, (f) eddy viscosity into the film determines the velocity distribution into the film, (g) unidirectional mass transfer, and (h) equilibrium condition at the interface. According to the profile of the eddy transport coefficients, it investigated several proposals, but it was found that most of the authors employed the van Driest [71] equation for calculating the eddy viscosity profile near the wall tube. However, near the interface, the authors supposed damped turbulence, in which the mass transport takes place only near the interface [24].

Regarding to the Nusselt number, the numerical results that were computed using various eddy transport coefficients were higher than the experimental results in Yüksel and Schlünder [2], however, the numerical mass transfer coefficient agreed well with the experimental study because the assumption of the turbulence model that considered the damping effect (near the wall and near the interface) was suitable. In addition, they suggested a new dimensionless group

to describe the effect of the thermophysical properties in the Nusselt number.

Patnaik and Perez-Blanco [28] investigated the simultaneous heat and mass transfer in the absorption process for the wavy film flow, employing an iterative finite-difference method for a transient and two-dimensional (2-D) model, testing the operation conditions such as (a) inlet concentration of 60%, (b) absorption pressure of $0.850kPa$, (c) inlet temperature solution of $40°C$, (d) surface temperature of $35°C$, and (e) wavy-laminar regime $200 \leq Re \leq 1000$, in which there are two types of wavy laminar. The mass transfer rate was found to be higher in wavy laminar than in smooth laminar regime due to the inertial and roll waves it promotes, enhancing the normal convective flux.

$$Nu = \delta Re_l Pr_l \left[(T_i - T_o) + \left(\frac{x_i - x_o}{x_o} \right) \frac{i_{abs}}{c_{p,l}} \right] (4L\Delta T_{lm})^{-1} \tag{60}$$

$$Sh = \delta Re_l Sc_l \left((x_i - x_o) \right) (4Lx_o \Delta x_{lm})^{-1} \tag{61}$$

Takamatsu et al. [29] studied the heat and mass transfer behavior in a $400mm$ long falling vertical in-tube absorber, comparing the results with the previously reported $1200mm$ long, in which the effect of the solution flow rate ($0.013 - 0.025kg\ s^{-1}$), solution subcooling temperature ($\Delta T_{sub} = 0°C$ and $\Delta T_{sub} = 5°C$), and cooling water temperature ($T_{l,i} = 34; 35°C$) were tested. The experimental work found the total wettability of the tube when the Reynolds number reached $Re = 130$. Nevertheless, the film break-down may happen below this value, causing the deterioration of the average heat and mass transfer coefficient. In addition, it pointed out that the logarithmic mean difference in concentration is not always valid for the absorber, diverging from the real driving force of the absorption process. According to the absorption process, when the solution was fed at the saturated condition ($\Delta T_{sub} = 0°C$), the absorption process started after the thermal boundary layer on the cooled wall reaching the vapor-liquid interface, and for the subcooled condition, the absorption process began in the inlet of the absorber. The higher absorption process was given at the first $400mm$ $(15 - 50\%)$ when compared with the last $800mm$ section, explained due to the wettability problems, such as the breaking

film. This allows concluding that the absorption process was deeply influenced by the tube length [29].

5.2. Works involving falling film technology

Nosoko et al. [25] carried out an experimental study of oxygen gas absorption in falling water films over horizontal tubes in the laminar regime $(10 - 150)$. There was a complete tube wettability without additives, using copper tubes and a capillary tube of distribution. It tested various tube spacings $(2, 5, 10$ and $15mm)$ and flow rates, in which an isothermal film was assumed due to the low heat of absorption of the oxygen. The logarithmic mean concentration difference and the equilibrium condition at the interface were used to calculate the mass transfer coefficient, in which all the tests were developed in atmospheric pressure, and the temperature ranged between $18 - 23°C$.

It was concluded that the droplet flow promotes more increase of the mass transfer than the sheet droplet because it penetrates the film depth, enhancing the mass transfer coefficient at the wall-film interface, and the mass transfer could improve up to 45%, on the Reynolds number $30 - 150$. On the other hand, the Sherwood number improved when the tube spacing increased from 2 to $5mm$, and it was kept constant for higher tube spacing, such as higher than 10 [25]. The following correlations were obtained:

$$Sh = 0.03777 Re_l^{0.86} Sc_l^{0.5} \tag{62}$$

NH3 Goel and Goswami [72] [73] used the Wilke correlation [43] to compute the heat transfer cofficient for the laminar flow regime, in which Wilke [43] studied the falling film heat transfer, and Kandlikar [74] showed the next follows, For $Re \leq 2460 Pr^{-0.646}$

$$Nu = 1.92 Re^{-1/3} \tag{63}$$

For $2460 Pr^{-0.646} \leq Re \leq 1600$

$$Nu = 0.0323 Re^{1/5} Pr^{0.344} \tag{64}$$

For $1600 \leq Re \leq 3200$

$$Nu = 0.00102 Re^{2/3} Pr^{0.344} \tag{65}$$

For $3200 \leq Re$

$$Nu = 0.0087 Re^{2/5} Pr^{0.344} \tag{66}$$

Takamatsu [29] showed that Chun and Seban [52] may be used for Reynolds number higher than Re=150. However, Chun and Seban [52] superestimates the Nusselt number, in which Chun and Seban [52], [75] Laminar regime, $Re \leq 2.44 Ka^{-1/11}$ is given by

$$Nu = 0.822 Re^{-1/3} \tag{67}$$

Wavy laminar regime, $2.44 Ka^{-1/11} \leq Re \leq 5800 Pr^{-1.06}$

$$Nu = 0.822 Re^{-0.22} \tag{68}$$

Turbulent regime, and the departure from the wavy laminar to turbulent regime $Re = 5800 Pr^{-1.06}$

$$Nu = 0.0038 Re^{0.4} Pr^{0.65} \tag{69}$$

Hu and Jacobi [44], sheet mode

$$Nu = 2.194 Re^{0.28} Pr^{0.14} Ar^{-0.20} \left(\frac{S-D}{D} \right)^{0.07} \tag{70}$$

Jet mode, and the departure from the jet mode to the sheet mode is $Re = 1.431 Ga^{0.234}$.

$$Nu = 1.378 Re^{0.242} Pr^{0.26} Ar^{-0.23} \left(\frac{S-D}{D} \right)^{0.08} \tag{71}$$

Droplet mode, and the departure from the droplet mode to the jet is $Re = 0.084 Ga^{0.302}$.

$$Nu = 0.113 Re^{0.85} Pr^{0.85} Ar^{-0.27} \left(\frac{S-D}{D} \right)^{0.04} \tag{72}$$

Alhusseini et al. [76], Laminar regime

$$Nu = 2.65 Re^{-0.158} Ka^{0.0563} \tag{73}$$

Turbulent regime,

$$Nu = \frac{Pr\delta^{*1/3}}{A_1 Pr^{3/4} + A_2 Pr^{1/2} + A_3 Pr^{1/4} + C_1 + B_1 Ka^{1/2} Pr^{1/2}} \tag{74}$$

where

- $A_1 = 9.17$
- $A_2 = 0.328\pi(130 + \delta^*)$
- $A_3 = 0.289(152100 + 2340\delta^* + 7\delta^{*2})/\delta^{*2}$;
- $B_1 = (2.51x10^6\delta^{*1/3}Ka^{-0.173})/Re^{(3.49Ka^{0.0675})}$
- $C_1 = 8.82 + 0.0003Re$
- $\delta^* = 0.0946Re^{0.8}$;

Shahzada et al. [77] modified the Han and Flecter's correlation, getting;

$$Nu = 0.0017\left(\frac{\nu^2}{gk^3}\right)^{-0.276} Re^{-1/3} Pr^{-0.75}\left[2e^{S/S_o} - 1\right]^{0.07}\left(\frac{T_{sat}}{322}\right)^{0.73} \tag{75}$$

and the modified of Chun and Seban's correlation [52], getting;

$$Nu = 0.20\left(\frac{\nu^2}{gk^3}\right)^{0.23} Re^{1.66}\left[2e^{S/S_o} - 1\right]^{0.006}\left(\frac{T_{sat}}{319}\right)^{-1.01} \tag{76}$$

where, $S_o = 30000ppm$, while S is the salt concentration given in ppm, T_{sat} is the saturation temperature given in K.

Parken et al. [78], for the $25.4mm$ diameter tube.

$$Nu = 0.042Re^{0.15} Pr^{0.53} \tag{77}$$

for the $50.8mm$ diameter tube.

$$Nu = 0.038Re^{0.15} Pr^{0.53} \tag{78}$$

Mitrovic [53], for $160 \leq Re \leq 560$

$$Nu = 0.01374Re^{0.349} Pr^{0.5}\beta \tag{79}$$

where, $\beta = \frac{(S/D)^{0.158}}{1+e^{0.008Re^{1.32}}}$

Liu et al. [79] for $1.75 \leq Pr \leq 7.02$; $800 \leq Re \leq 5000$; $213 \leq Ar \leq 1546$; $10mm \leq D \leq 40mm$,

$$Nu = 0.041 Re^{0.3} Pr^{0.66} Ar^{-0.12} \tag{80}$$

Chien [80] for R-245fa, $6.26 \leq Pr \leq 7.15$; $115 \leq Re \leq 372$; $0.000165 \leq We \leq 0.000168$

$$Nu = 0.0386 Re^{0.09} Pr^{0.986} \tag{81}$$

Narváez-Romo and Simões-Moreira [81] for water, $0.72 \leq Pr \leq 7.92$; $160 \leq Re \leq 940$

$$Nu = 0.21 Re^{-0.067} Pr^{0.528} \tag{82}$$

Leite [82] developed a numerical study of both absorber and generator, applying the finite difference method for an inclined plate, in which the mass, species and energy balances were employed. Both components were modeled for various operation conditions, testing the geometry dimensions, plate angle of inclination, wall temperature and the inlet conditions. The results confirmed that the vertical position is the best position of performance, promoting a stable operation condition. Finally, it found a correlation to correlate the heat and mass transfer over an inclined plate as a function of the vertical position, given by:

$$F_{Nu}(\beta) = \frac{Nu(\beta)}{Nu(\pi/2)} \tag{83}$$

$$F_{Sh}(\beta) = \frac{Sh(\beta)}{Sh(\pi/2)} \tag{84}$$

$$F_{Nu}(\beta) = e^{-0.081(\beta-\pi/2)+0.054(\beta^2-\pi^2/4)-0.012(\beta^3-\pi^3/8)} \tag{85}$$

$$F_{Sh}(\beta) = e^{-1.712(\beta-\pi/2)+1.402(\beta^2-\pi^2/4)-0.392(\beta^3-\pi^3/8)} \tag{86}$$

These factors were obtained by fitting the numerical results of Karami and Farhanieh [23]. In addition, the correlation of Kang et al. [27] was used to compute the heat and mass transfer coefficient for the vertical position ($\beta = \pi/2$).

Cerezo et al. [33] studied the absorption process using a corrugated plated heat exchanger with three channels (effective surface area of $0.1m^2$), evaluating the mean parameters that affect the absorption performance. Tests were ranged for absorption rate flux from 0.0025 to $0.0063kg\ m^{-2}s^{-1}$, solution heat transfer coefficient from 2700 to 5400 $W\ m^{-2}\ ^{\circ}C^{-1}$, and an absorber thermal load from 0.5 to $1.3kW$. The heat transfer coefficient increased almost linearly when the solution flow rate increased due to the turbulent effect over the thermal layer on the surface (a reduction). On the other hand, the Reynolds number changes did not affect the mass absorption rate flux when the inlet concentration was 33%. Moreover, a smaller concentration (between 29% and 33%) presented higher mass absorption rate flux for the same Reynolds number ($Re = 290$), being an opposite behavior to the driving force definition. In addition, the heat transfer coefficient decreased when the cooling water temperature decreased. Finally, the highest heat transfer rate and mass absorption rate flux were reached for higher values of absorption pressure.

Next, an analysis of the heat and mass transfer behavior was carried out, in which all the previous correlations (Nusselt and Sherwood numbers) were evaluated and compared each other based on modeling and simulation of an ARC, obtaining a possible heat and mass transfer mapping for refrigeration and air-conditions applications.

6. Heat and mass transfer mapping for refrigeration and air-conditioning applications

Ammonia-water ($NH_3 - H_2O$) and lithium bromide-water ($LiBr - H_2O$) ARC have been simulated to find the typical operational conditions, in which the mass and energy equations, thermophysical properties of mixtures and mean operational parameters were implemented through the *Engineering Equations Solver* - EES). Therefore, for these conditions, the heat and mass transfer correlations were evaluated as is showed in Fig. (3).

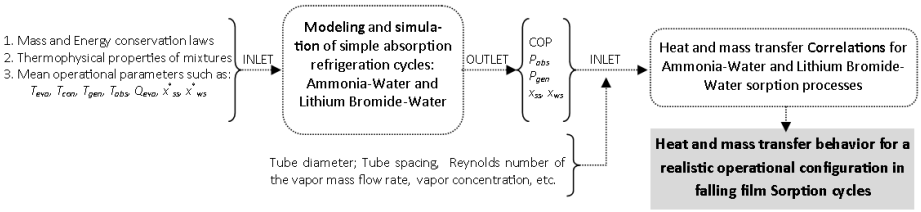

Figure 3: Method to evaluate the heat and mass transfer coefficient in a realistic ARC

6.1. Modeling and simulation of ARC

An ARC modelization was carried out, taking into account all the components of the cycle such as generator, rectifier (for $NH_3 - H_2O$ only), condenser, expansion valves, evaporator, absorber, and pump. Each one was analyzed as an independent control volume, in which the mass, species and energy equations were developed in a steady-stage regime. Next, the ammonia-water ARC will be analyzed.

6.1.1. Ammonia-water ARC

ARC modelization requires deep attention at the most critical processes such as generation and absorption processes due to simultaneous heat and mass transfer. Therefore, these components are analyzed as is shown in Fig. (4).

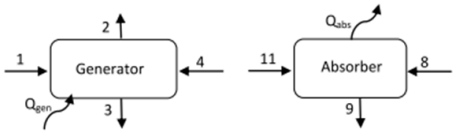

Figure 4: Control volume for the generation and the absorption process

The falling film generator is employed to separate the ammonia (2-label) from the ammonia-water strong solution (1-label) when a heat source is applied (Q_{gen}), in which the weak solution is the remaining solution after the separation process (3-label). The rectifier is used to purify the ammonia vapor and hence that condensed goes back to the generator (4-label). On the other hand, the falling film absorber is used to absorb the ammonia vapor coming of the evaporator (8-label) into the weak ammonia-water solution (11-label) that comes

of the generator, and then the strong ammonia-water solution (9-label) is obtained, as shown in Fig. (4), in which the (Q_{abs}) is rejected to the coolant fluid. The mass, ammonia mass, and energy equations are given by Eqs. (87-89) and by Eqs. (90-92) for the generation and absorption processes, respectively; while $\dot{m}$, i and x are the mass flow rate, specific enthalpy and the ammonia mass fraction, respectively.

$$\dot{m}_3 + \dot{m}_2 = \dot{m}_1 + \dot{m}_4 \tag{87}$$

$$\dot{Q}_{gen} = \dot{m}_2 i_2 + \dot{m}_3 i_3 - \dot{m}_1 i_1 - \dot{m}_4 i_4 \tag{88}$$

$$\dot{m}_3 x_3 + \dot{m}_2 x_2 = \dot{m}_1 x_1 + \dot{m}_4 x_4 \tag{89}$$

$$\dot{m}_{11} + \dot{m}_8 = \dot{m}_9 \tag{90}$$

$$\dot{Q}_{abs} = \dot{m}_8 i_8 + \dot{m}_{11} i_{11} - \dot{m}_9 i_9 \tag{91}$$

$$\dot{m}_{11} x_{11} + \dot{m}_8 x_8 = \dot{m}_9 x_9 \tag{92}$$

Several simplified hypothesis were carried out to solve the whole equation system such as; (1) condensation temperature, $T_{con} = 40°C$; (2) evaporation temperature, $T_{eva} = 7°C$; (c) thermal load, $\dot{Q}_{eva} = 3.517kW$[2]; (d) generation temperature, $T_{gen} = 100°C$, and (e) absorption temperature, $T_{abs} =°\ C$. In addition, other assumptions were carried out to simplify the system, (a) quality equal to $q_u = 0$ - saturated liquid- in the 3, 4, 6 and 9 points; (b) quality equal to $q_u = 1$ saturated vapor- in the 2, 5 and 8 points; (b) two pressure levels only: high pressure level in the 1, 2, 3, 4, 5, 6, 11 and 12, low pressure level

[2]Thermal load was necessary to run the model, however, the thermal load affect directly the equipment size

in the 7, 8, 9 and 10 points; (c) generation process occurs in thermodynamic equilibrium, $T_3 = T_2$; (d) the temperature in the point 4 is computed by the arithmetic mean, $T_4 = 0.5 * (T_2 + T_5)$ [83], (e) heat exchanger with infinity area, $Q_{subcool} = Q_{pre-heat}$, $T_{11} = T_{12}$, and (f) isentropic pumping. Fig. (5) shows the numerical results of the whole operational parameters such as ammonia-mass fraction (x), absorption pressure (P_{abs}) and generation pressure (P_{gen}), mass flow rate ($\dot{m}$), just to mention a few.

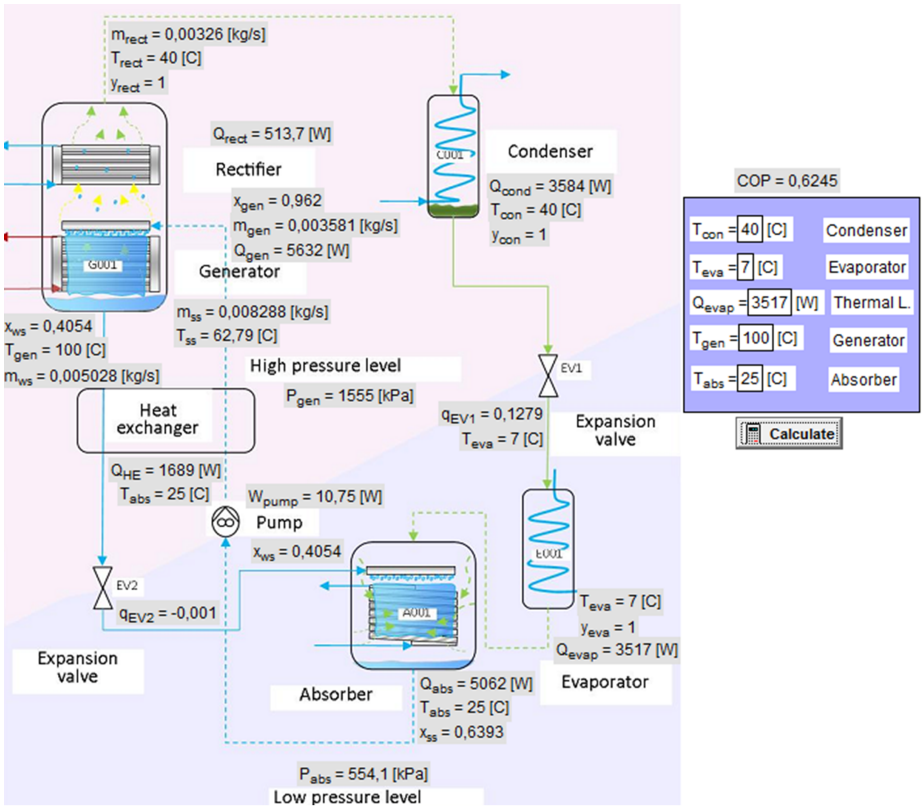

Figure 5: Results of the simulation of the ammonia-water ARC

However, some parameters have been adjusted to cover the operation ranges applied in refrigeration/air conditioning systems. The simulation was carried out for two evaporation temperatures; $T_{eva} = -20°C$ for refrigeration applications and $T_{eva} = 7°C$ for air condition systems, two condensation temper-

Table 7: Operational conditions of the ammonia-water ARC

Cond.	$T_{con}, ^\circ C$	$T_{eva}, ^\circ C$	$T_{gen}, ^\circ C$	COP	P_{abs}, kPa	P_{gen}, kPa	$x_{ss}, \%$	$x_{ws}, \%$	Pr	Sc
1	40	7	100	0.6245	554.1	1555	63.72	40.52	1.64	14.4
2	40	7	110	0.5157	554.1	1555	63.72	31.41	1.91	21.5
3	40	-20	100	0.5547	190.1	1555	41.51	40.52	2.29	37.3
4	40	-20	110	0.4606	190.1	1555	41.51	31.41	2.63	52.4
5	30	7	100	0.6083	554.1	1167	63.72	34.54	1.82	18.9
6	30	7	110	0.4779	554.1	1167	63.72	25.78	2.1	27.4
7	30	-20	100	0.5407	190.1	1167	41.51	34.54	2.52	46.9
8	30	-20	110	0.4298	190.1	1167	41.51	25.78	2.87	64.2

atures ($T_{con} = 40^\circ C$ and $T_{con} = 30^\circ C$), and two generation temperatures ($T_{gen} = 100^\circ C$ and $T_{gen} = 110^\circ C$), aiming to achieve typical operation conditions. All the simulation results are showed in Table (7), in which eight operation conditions were evaluated and showed at the first. The second, third and forth columns show the condensation temperature (T_{con}), evaporation temperature (T_{eva}) and generation temperature T_{gen}, respectively; while, COP, P_{abs} and P_{gen} are the coefficient of performance, absorption pressure and generation pressure, respectively; Next, x_{ss}, x_{ws} are the strong and weak solution, respectively. Finally, the last two columns show the Prandtl number (Pr) and Schmidt number (Sc) for the absorption conditions.

6.1.2. Lithium bromide-water ARC

For lithium bromide-water working fluid, the operation conditions were also defined by the same previous analysis. The results are showed in Fig. (6), in which the lithium bromide concentrations were defined at the design specifications using the crystallization limit to define the weak solution concentration. The generator temperature was declared as a function of the weak and strong liquid concentration, turning out as a dependent variable. Evaporation temperature was only evaluated at $7^\circ C$ due to refrigerant properties (water). Therefore, this technology is widely used in air conditioning applications. All the results are showed in Tab. (**??**), in which two operation conditions were evaluated and showed in the first column, the second and third columns show the condensa-

tion temperature (T_{con}) and evaporation temperature (T_{eva}), respectively; while x_{ss}, x_{ws} are the strong and weak solution, respectively. Next, the coefficient of performance (COP), absorption pressure (P_{abs}), generation pressure (P_{gen}), generation temperature (T_{gen}). Finally, the Prandtl number (Pr) and Schmidt number (Sc) are computed.

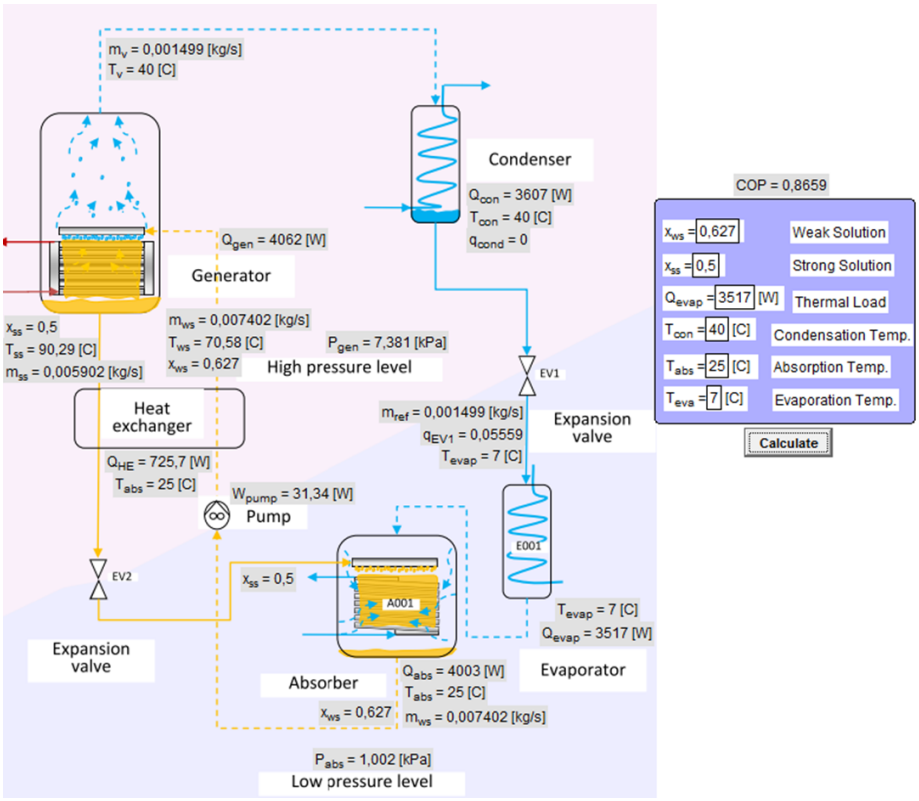

Figure 6: Results of the simulation of the lithium bromide-water ARC

6.2. Heat and mass transfer mapping

6.2.1. Ammonia-water working fluid

Fig. (7) shows the Sherwood number as a function of the Reynolds number, whose mass transfer is enhanced as the Reynolds number is increased. However, the mass transfer coefficient will strongly enhance as the absorption refrigeration cycle achieves evaporation temperatures below $0°C$. Moreover, Fig. (7)

displays the possible mass transfer mapping for the ARC for the whole operational conditions given in Tab. (7). The mass transfer mapping from Bohra [31] agree with Lee [37]. However, Kang et al. [27] underestimates these values, in which it may be explained by the conditions that the experiments were carried out at the test rig (low purity of ammonia vapor). Therefore, the Sherwood number in refrigeration/air conditioning applications may vary from 0.015 to 0.08. The operational conditions 2 to 7 were not shown in Fig. (7), but these values are found in Tab. (7), and in Tab. (2) the application range of these correlations are displayed.

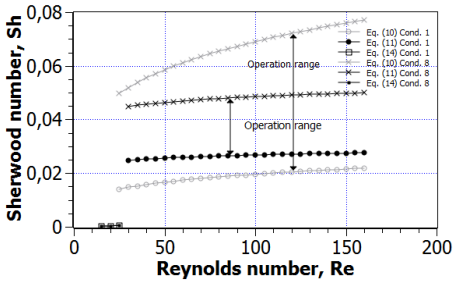

Figure 7: Sherwood number as a function of the Reynolds number for the ammonia-water solution

Fig. (8) shows the Nusselt number as a function of the Reynolds number. The first Fig. (upper-left side) displays the correlations used in the falling film technology using other working fluids for an evaporation process, in which these correlations such as Narváez-Romo and Simões-Moreira [81], Zavaleta-Aguilar and Simões-Moreira[36], Wilke [43] and Alhusseini et al. [76] show similar heat transfer values from Bohra [31] for the Reynolds numbers between 100 and 150. However, the fashion curves of these processes are opposite. The second Fig. (upper-right side) displays a comparison between Jeong et al. [15], Kwong and Jeong [14], Lee et al. [41] and Hu and Jacobi [49], showing that these correlations present similar results each other, i.e., Kwong and Jeong [14] correlation found inside the operating range of Lee et al. [41] and Hu and Jacobi [49]. Therefore, the Hu and Jacobi [49] correlation may be used to design the absorption process

(droplet-column pattern flow). However, Jeong et al. [15] underestimates the heat transfer due to this correlation neglects the effects taken into account by the Prandtl number. The third Fig. (bottom-left side) compares the correlations of Kwong and Jeong [14], Lee [37], Jeong et al. [15], and Kang et al. [27], showing the behavior of the Nusselt number for low Reynolds numbers (10 to 50). Kang et al. [27] underestimates the Nusselt number as the Reynolds number increases. Finally, the last Fig. (bottom-right side) compares the correlation of Jeong et al. [15], Kwong and Jeong [14], Lee [37] and Hu and Jacobi [49], in which all the correlations have a good agreement. Therefore, Fig. (8) shows that the Nusselt number may be vary between 0.001 and $0,2$ for the Reynolds number ranged from 10 to 250 (with an exception of Bohra [31]). It is worthwhile to mention that the best performance of the heat transfer is achieved at the lowest evaporation temperature ($T_{eva} = -20°C$) for all the correlations.

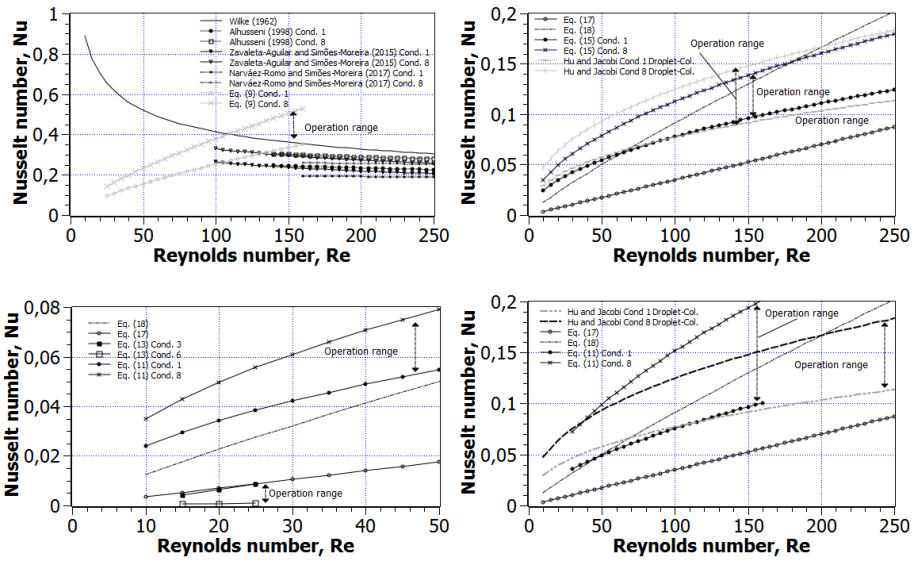

Figure 8: Nusselt as a function of the Reynolds number for the ammonia-water solution

6.2.2. Lithium bromide-water working fluid

Fig. (9) shows the Sherwood number as a function of the Reynolds number, in which the correlations display different behavior for the same operational conditions, i.e., Karami and Farhanieh [22] and Karami and Farhanieh [23] show a strong dependence of the Sherwood number as the Reynolds number changes, enhancing the mass transfer as the Reynolds number increases. In contrast, Kim and Ferreira [32] show that the increase of the Reynolds number diminishes the Sherwood number. It is worthwhile to mention that the Kim and Ferreira [32] correlations were experimentally obtained. On the other hand, Babadi and Farhanieh [59] underestimates the Sherwood number as compared with Kim and Ferreira [32], Karami and Farhanieh [22] and Karami and Farhanieh [23]. Fig. (10) shows the behavior of the Nusselt number as a function of the Reynolds number, in which the heat transfer improves as the Reynolds number increases. Nevertheless, the correlations of Babadi and Farhanieh [59], and Karami and Farhanieh [22] shows an opposite behavior.

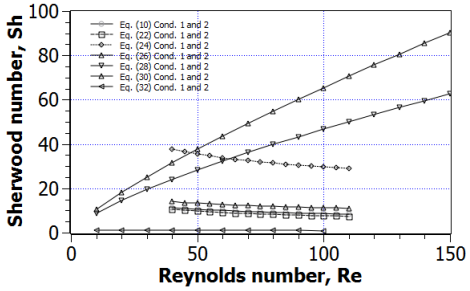

Figure 9: Sherwood number as a function of the Reynolds number for the Lithium bromide-water solution

7. Conclusion

In this communication, a review study on heat and mass transfer correlations is presented. The transfer correlations deal with sorption machine using falling film technology with ammonia-water solution or lithium bromide-water solution. The review summarizes the operating range of each correlations within

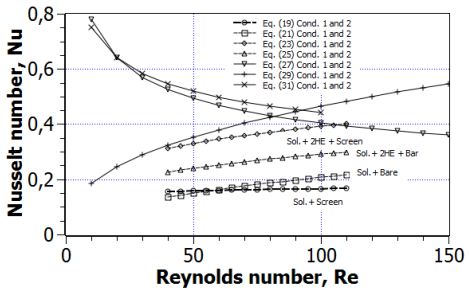

Figure 10: Nusselt number as a function of the Reynolds number for the Lithium bromide-water solution

tables, as well as the specific configuration related to each correlation. A graphical comparison of the transfer correlations is performed for a given operation condition. The fact that the transfer correlations may behave differently calls for further study, specifically to implement the correlations into a *more realistic operational* configurations related to the sorption machine.

8. Acknowledgements

The first author thanks to COLCIENCIAS and CNPq for the financial support.

9. References

References

[1] M. Carmo Elvas, M. I. Perez, S. Carvalho, Making science cooler: Carré's apparatus, in: Int. Conference of ESHS, 2010, pp. 441–449.

[2] M. Yüksel, E. Schlünder, Heat and mass transfer in non-isothermal absorption of gases in falling liquid films, Chem. Eng. Process. Process Intensification 22 (4) (1987) 193–202.

[3] T. Fujita, Falling liquid films in absorption machines, Int. J. Refrigeration 16 (4) (1993) 282–294.

[4] J. Castro, C. Oliet, I. Rodríguez, A. Oliva, Comparison of the performance of falling film and bubble absorbers for air-cooled absorption systems, Int. J. Thermal Sciences 48 (7) (2009) 1355–1366.

[5] J. R. Thome, Falling film evaporation: state-of-the-art review of recent work, J. Enhanced Heat Transfer 6 (1999) 263–278.

[6] J. D. Killion, S. Garimella, A critical review of models of coupled heat and mass transfer in falling-film absorption, International Journal of Refrigeration 24 (8) (2001) 755–797.

[7] G. Ribatski, A. M. Jacobi, Falling-film evaporation on horizontal tubes - A critical review, Int. J. Refrigeration 28 (5) (2005) 635–653.

[8] B. Narváez-Romo, J. R. Simões-Moreira, Falling film evaporation: a qualitative analysis of the distribuition system, in: Proceeding of the Brazilian Congress of Thermal Sciences and Eng. (ENCIT), Belém, 2014.

[9] J. S. Prost, M. T. González, M. J. Urbicain, Determination and correlation of heat transfer coefficients in a falling film evaporator, J. of Food Eng. 73 (4) (2006) 320–326.

[10] B. Narváez-Romo, J. R. Simões-Moreira, Falling Film Evaporation: an Overview, in: Proceeding of 22nd Int. Congress of Mechanical Eng. (COBEM), Riberão Preto, 2013, pp. 1–7.

[11] C. Tomforde, A. Luke, Experimental Investigations on Falling-Film Absorbers with Horizontal Tubes a Review, International Refrigeration and Air Conditioning Conference at Purdue (2011) (2012) 2166.

[12] A. M. Abed, M. Alghoul, M. H. Yazdi, A. N. Al-Shamani, K. Sopian, The role of enhancement techniques on heat and mass transfer characteristics of shell and tube spray evaporator: a detailed review, Applied Thermal Engineering 75 (2015) 923–940.

[13] R. Taylor, R. Krishna, Multicomponent mass transfer, Vol. 2, John Wiley & Sons, 1993.

[14] K. Kwon, S. Jeong, Effect of vapor flow on the falling-film heat and mass transfer of the ammonia/water absorber, Int. J. Refrigeration 27 (8) (2004) 955–964.

[15] S. Jeong, S. K. Lee, K.-K. Koo, F. Ziegler, et al., Heat transfer performance of a coiled tube absorber with working fluid of ammonia/water/discussion, ASHRAE Transactions 104 (1998) 1577.

[16] G. Florides, S. Kalogirou, S. Tassou, L. Wrobel, Design and construction of a libr–water absorption machine, Energy Conversion and Management 44 (15) (2003) 2483–2508.

[17] I. Fujita, E. Hihara, Heat and mass transfer coefficients of falling-film absorption process, Int. J. Heat Mass Transfer 48 (13) (2005) 2779 – 2786.

[18] M. R. Islam, N. Wijeysundera, J. Ho, Evaluation of heat and mass transfer coefficients for falling-films on tubular absorbers, Int. J. Refrigeration 26 (2) (2003) 197–204.

[19] T. H. Chilton, A. P. Colburn, Mass transfer (absorption) coefficients prediction from data on heat transfer and fluid friction, Industrial & Eng. Chemistry 26 (11) (1934) 1183–1187.

[20] E. Treybal Robert, Mass-transfer operations, McGraw-Hill Book Company, 1981.

[21] W. Nusselt, Die oberflachenkondesation des wasserdamffes the surface condensation of water, Zetrschr. Ver. Deutch. Ing. 60 (1916) 541–546.

[22] S. Karami, B. Farhanieh, A numerical study on the absorption of water vapor into a film of aqueous LiBr falling along a vertical plate, Heat and Mass Transfer/Waerme- und Stoffuebertragung 46 (2) (2009) 197–207.

[23] S. Karami, B. Farhanieh, Numerical modeling of incline plate LiBr absorber, Heat and Mass Transfer/Waerme- und Stoffuebertragung 47 (3) (2011) 259–267.

[24] M. Yüksel, E. Schlünder, Heat and mass transfer in non-isothermal absorption of gases in falling liquid films Part II: Theoretical description and numerical calculation of turbulent falling film heat and mass transfer, Chem. Eng. Process: Process Intensification 22 (4) (1987) 203–213.

[25] T. Nosoko, a. Miyara, T. Nagata, Characteristics of falling film flow on completely wetted horizontal tubes and the associated gas absorption, Int. J. Heat Mass Transfer 45 (13) (2002) 2729–2738.

[26] C. Ferreira, C. Keizer, C. Machielsen, Heat and mass transfer in vertical tubular bubble absorbers for ammonia-water absorption refrigeration systems, Int. J. Refrigeration 7 (6) (1984) 348–357.

[27] Y. T. Kang, A. Akisawa, T. Kashiwagi, Experimental correlation of combined heat and mass transfer for NH3-H2O falling film absorption, Int. J. Refrigeration 22 (1999) 250–262.

[28] V. Patnaik, H. Perez-blanco, A Study of Absorption Enhancement by Wavy Film Flows, Int. J. Heat Fluid Flow 17 (1996) (1996) 71–77.

[29] H. Takamatsu, H. Yamashiro, N. Takata, H. Honda, Vapor absorption by LiBr aqueous solution in vertical smooth tubes, Int. J. Refrigeration 26 (6) (2003) 659–666.

[30] S. Jani, M. H. Saidi, a. a. Mozaffari, Tube bundle heat and mass transfer characteristics in falling film absorption generators, Int. Commun. Heat Mass 30 (4) (2003) 565–576.

[31] L. K. Bohra, Analysis of binary fluid heat and mass transfer in ammonia-water absorption, Ph.D. thesis, Georgia Institute of Technology (2007).

[32] D. S. Kim, C. a. Infante Ferreira, Flow patterns and heat and mass transfer coefficients of low Reynolds number falling film flows on vertical plates: Effects of a wire screen and an additive, Int. J. Refrigeration 32 (1) (2008) 138–149.

[33] J. Cerezo, M. Bourouis, M. Vallès, A. Coronas, R. Best, Experimental study of an ammoniawater bubble absorber using a plate heat exchanger for absorption refrigeration machines, Appl. Thermal Eng. 29 (5-6) (2009) 1005–1011.

[34] C. Shi, C. Xu, H. Hu, Y. Ying, Study on falling film generation heat transfer of lithium bromide solution in vertical tubes, J. of Thermal Science 18 (3) (2009) 241–245.

[35] C. Shi, Q. Chen, T.-C. Jen, W. Yang, Heat transfer performance of lithium bromide solution in falling film generator, Int. J. Heat Mass Transfer 53 (15-16) (2010) 3372–3376.

[36] E. Zavaleta-Aguilar, J. Simões-Moreira, Horizontal tube bundle falling film distiller for ammonia–water mixtures, Int. J. Refrigeration 59 (2015) 304–316.

[37] S. Lee, Development of techniques for in-situ measurement of heat and mass transfer in ammonia-water absorption systems, Ph.D. thesis, Georgia Institute of Technology (2007).

[38] V. E. Nakoryakov, N. I. Grigoryeva, M. V. Bartashevich, Heat and mass transfer in the entrance region of the falling film: Absorption, desorption, condensation and evaporation, International Journal of Heat and Mass Transfer 54 (21-22) (2011) 4485–4490.

[39] R. L. Cerro, S. Whitaker, Entrance region flows with a free surface: the falling liquid film, Chemical Engineering Science 26 (6) (1971) 785–798.

[40] X. Peng, B. Wang, G. Peterson, H. Ma, Experimental investigation of heat transfer in flat plates with rectangular microchannels, International Journal of Heat and Mass Transfer 38 (1) (1995) 127–137.

[41] K. B. Lee, B. H. Chun, J. C. Lee, C. H. Lee, S. H. Kim, Experimental analysis of bubble mode in a plate-type absorber, Chem. Eng. Sci. 57 (11) (2002) 1923–1929.

[42] S. Lee, L. K. Bohra, S. Garimella, A. K. Nagavarapu, Measurement of absorption rates in horizontal-tube falling-film ammonia-water absorbers, International Journal of Refrigeration 35 (3) (2012) 613–632.

[43] W. Wilke, (heat transfer to falling liquid films) warmeubertragung an rieselfilme, VDI-Forschungsheft 490 (1962) 36.

[44] X. Hu, A. Jacobi, The intertube falling film: Part 2mode effects on sensible heat transfer to a falling liquid film, J. Heat Transfer 118 (3) (1996) 626–633.

[45] J. M. Meacham, S. Garimella, Ammonia-water absorption heat and mass transfer in microchannel absorbers with visual confirmation., ASHRAE Transactions 110 (1).

[46] X. Daguenet-Frick, P. Gantenbein, J. Müller, B. Fumey, R. Weber, Seasonal thermochemical energy storage: Comparison of the experimental results with the modelling of the falling film tube bundle heat and mass exchanger unit, Renewable Energy.

[47] K. B. Lee, B. H. Chun, J. C. Lee, J. C. Hyun, S. H. Kim, Comparison of heat and mass transfer in falling film and bubble absorbers of ammonia water (September 2001) (2002) 191–205.

[48] A. Dorokhov, V. Bochagov, Heat transfer to a film falling over horizontal cylinders, Heat transfer. Soviet research 15 (2) (1983) 96–101.

[49] X. Hu, A. Jacobi, The intertube falling film: Part 1flow characteristics, mode transitions, and hysteresis, J. Heat Transfer 118 (3) (1996) 616–625.

[50] J. Meacham, S. Garimella, Experimental demonstration of a prototype microchannel absorber for space-conditioning systems, in: Int. Sorption Heat Pump Conference, Shanghai, China, 2002, pp. 270–276.

[51] J. M. Meacham, S. Garimella, Ammonia-water absorption heat and mass transfer in microchannel absorbers with visual confirmation., ASHRAE Transactions 110 (1).

[52] K. Chun, R. Seban, Heat transfer to evaporating liquid films, J. Heat Transfer 93 (4) (1971) 391–396.

[53] J. Mitrovic, Influence of tube spacing and flow rate on heat transfer from a horizontal tube to a falling liquid film, in: Proceedings of the 8th Int. Heat Transfer Conference, Vol. 4, 1986, pp. 1949–1956.

[54] W. Owens, Correlation of thin film evaporation heat transfer coefficients for horizontal tubes, 1978.

[55] Y. Fujita, M. Tsutsui, Experimental investigation of falling film evaporation on horizontal tubes, Heat Transfer-Japanese Research 27 (8) (1998) 609–618.

[56] M. Conde, Thermo-physical properties of {NH3+H2O} mixtures for industrial design of absorption refrigeration equipment, M. Conde Eng., Zurich (2006) 12–15.

[57] S. Jani, Simulation of Heat and Mass Transfer Process in Falling Film Single Tube Absorption Generator, Int. J. of Science and Eng. Investigations 1 (3) (2012) 79–84.

[58] McNeely LA, Thermodynamic properties of aqueous solutions of lithium bromide, ASHRAE 85 (1979) 413–434.

[59] F. Babadi, B. Farhanieh, Characteristics of heat and mass transfer in vapor absorption of falling film flow on a horizontal tube, Int. Commun. Heat Mass 32 (9) (2005) 1253–1265.

[60] K. Banasiak, J. Kozioł, Mathematical modelling of a LiBrH2O absorption chiller including two-dimensional distributions of temperature and concentration fields for heat and mass exchangers, International Journal of Thermal Sciences 48 (9) (2009) 1755–1764. doi:10.1016/j.ijthermalsci.2009.01.018.

[61] D. Kim, M. H. Kim, Heat transfer enhancement characteristics for falling-film evaporation on horizontal enhanced tubes with aqueous libr solution, J. Enhanced Heat Transfer 6 (1) (1999) 61–69.

[62] S. Jani, M. H. Saidi, A. Heydari, A. A. Mozaffari, Second law based optimization of falling film single tube absorption generator, in: ASME 2002 Int. Mechanical Eng. Congress and Exposition, American Society of Mechanical Engineers, 2002, pp. 49–54.

[63] M. Medrano, M. Bourouis, A. Coronas, Absorption of water vapour in the falling film of water–lithium bromide inside a vertical tube at air-cooling thermal conditions, Int. J. Thermal Sciences 41 (9) (2002) 891–898.

[64] L. Hoffmann, I. Greiter, A. Wagner, V. Weiss, G. Alefeld, Experimental investigation of heat transfer in a horizontal tube falling film absorber with aqueous solutions of libr with and without surfactants, Int. J. Refrigeration 19 (5) (1996) 331–341.

[65] S.-M. Yih, K.-Y. Chen, Gas absorption into wavy and turbulent falling liquid films in a wetted-wall column, Chem. Eng. Comm. 17 (1-6) (1982) 123–136.

[66] Y. Nagaoka, N. Nishiyama, K. Ajisaka, M. Nakamura, N. Inoue, H. Yabase, E. Hihara, T. Saito, Absorber of absorption refrigerating machine (enhance-

ment of heat and mass transfer in falling film absorbers by surface configuration).(73), na, 1987.

[67] K. Kim, N. Berman, D. Chau, B. Wood, Absorption of water vapour into falling films of aqueous lithium bromide, Int. J. Refrigeration 18 (7) (1995) 486–494.

[68] D. Kim, C. I. Ferreira, A gibbs energy equation for libr aqueous solutions, Int. J. Refrigeration 29 (1) (2006) 36–46.

[69] R. DiGuilio, R. Lee, S. Jeter, A. Teja, Properties of lithium bromide–water solutions at high temperatures and concentrations–i. thermal conductivity, ASHRAE Trans 96 (1) (1990) 702–708.

[70] M. Gierow, A. Jernqvist, Measurement of mass diffusivity with holographic interferometry for H2O-NaOH and H2O-LiBr working pairs, in: Proceedings of the Int. Heat Pump Conference, AES, Vol. 31, 1993, pp. 525–532.

[71] E. R. Van-Driest, On Turbulent Flow Near a Wall, J. Aeronautical Sciences 23 (11) (1956) 1007–1011.

[72] N. Goel, D. Y. Goswami, A compact falling film absorber, Journal of Heat Transfer 127 (9) (2005) 957–965.

[73] N. Goel, D. Y. Goswami, Analysis of a counter-current vapor flow absorber, International Journal of Heat and Mass Transfer 48 (7) (2005) 1283–1292.

[74] S. G. Kandlikar, Handbook of phase change: boiling and condensation, CRC Press, 1999.

[75] K. R. Chun, R. Seban, Performance prediction of falling-film evaporators, J. Heat Transfer 94 (4) (1972) 432–436.

[76] A. A. Alhusseini, K. Tuzla, J. C. Chen, Falling film evaporation of single component liquids, Int. J. Heat Mass Transfer 41 (12) (1998) 1623–1632.

[77] M. W. Shahzada, K. C. Ng, K. Thu, A. Myat, C. W. Gee, An improved film evaporation correlation for saline water at sub-atmospheric pressures, in: AIP Conference Proceedings, 2011.

[78] W. Parken, L. Fletcher, V. Sernas, J. Han, Heat transfer through falling film evaporation and boiling on horizontal tubes, J. Heat Transfer 112 (3) (1990) 744–750.

[79] Z.-H. Liu, Q.-Z. Zhu, Y.-M. Chen, Evaporation heat transfer of falling water film on a horizontal tube bundle, Heat Transfer-Asian Research 31 (1) (2002) 42–55.

[80] L.-H. Chien, Y.-L. Tsai, An experimental study of pool boiling and falling film vaporization on horizontal tubes in R-245fa, Appl. Thermal Eng. 31 (17) (2011) 4044–4054.

[81] B. Narváez-Romo, J. R. Simões-Moreira, Falling Liquid Film Evaporation in Subcooled and Saturated Water over Horizontal Heated Tubes, Heat Transfer Eng. (2016) 1–57.

[82] B. Leite, Modelagem do absorvedor e do gerador de ciclos de refrigeração por absorção de calor com o par NH3-H2O baseados na tecnologia de filme descendente sobre placas inclinadas, (In Portuguese) (2015).

[83] K. E. Herold, R. Radermacher, S. A. Klein, Absorption chillers and heat pumps, CRC press, 2016.